Magneto-electric multiferroics: designing new materials from *first-principles* calculations

Julien Varignon[1,2], Nicholas C. Bristowe[3], Eric Bousquet[1] and Philippe Ghosez[1]

[1]Theoretical Materials Physics, Q-MAT, CESAM, Université de Liège (B5), B-4000 Liège, Belgium

[2]Laboratoire CRISMAT, CNRS UMR 6508, ENSICAEN, Normandie Université, 6 Bd Maréchal Juin, F-14050 Caen Cedex 4, France

[3]School of Physical Sciences, University of Kent, Canterbury, CT2 7NH, UK

Abstract

In parallel with the revival of interest for magneto-electric multiferroic materials in the beginning of the century, *first-principles* simulations have grown incredibly in efficiency during the last two decades. Density functional theory calculations, in particular, have so become a must-have tool for physicists and chemists in the multiferroic community. While these calculations were originally used to support and explain experimental behaviour, their interest has progressively moved to the design of novel magneto-electric multiferroic materials. In this article, we mainly focus on oxide perovskites, an important class of multifunctional material, and review some significant advances to which contributed *first-principles* calculations. We also briefly introduce the various theoretical developments that were at the core of all these advances.

Although the magneto-electric effect, that allows the control of a magnetization (polarization) with an electric (magnetic) field and conversely, was proposed at the end of the 19th century by Pierre Curie[1], it only really started to be studied during the nineteen sixties and seventies, after Cr_2O_3 was proposed as good candidate by Landau and Lifshitz [2]. With our lives being more and more dependent on technology, the identification of multifunctional materials handling simultaneously large arrays of informations has become a real challenge for producing low energy consumption devices. Magneto-electric compounds thus received a considerable renewal of interest in the early 2000s[3] due to their potential for improved and new technological applications [4–7].

Before *first-principles* calculations became possible, identification of magneto-electric materials was typically guided by symmetry and thermodynamic considerations. According to thermodynamic requirements, the linear magneto-electric effect α is bound by the electric (χ^e) and magnetic (χ^m) susceptibilities through the formula $\alpha^2 < \chi^e.\chi^m$ [8]. Since ferroelectric (ferromagnetic) materials usually exhibit the largest electric (magnetic) susceptibilities, it is often expected that the linear magneto-electric effect α should be large in multiferroics, *i.e.* materials combining ferromagnetism and ferroelectricity. Nevertheless, the relationship between α, χ^e and χ^m is just an upper bound and there is in fact no guarantee that multiferroic materials will provide the largest magneto-electric effect. Strong coupling between the orders is an additional key ingredient.

The interest in multiferroic materials also owes its revival to the strong developments of *first-principles* simulations, most notably to Density Functional Theory (DFT). In the nineties, DFT became the standard platform for studying ferroelectricity in ABO_3 materials and it provided a deep understanding of the origin of ferroelectricity in $BaTiO_3$ and $PbTiO_3$[9]. Although originally restricted to explain experimental observations, the microscopic understanding enabled by DFT became a key tool for guiding experiments. For instance, DFT studies clarified ferroelectric and piezoelectric properties [9,10] or finite-size effects appearing in thin films [11–13]. As we will see in the examples tackled in this chapter, interest in magneto-electric compounds focused on ferroelectric

magnets and thus, it was natural to direct DFT studies of multiferroics. At the same time, strong advances in computer efficiency were also beneficial for enabling fast, reliable and large-scale studies.

As before for ferroelectricity, DFT initially served as a platform to explain the origin of multiferroism in systems such as in $BiFeO_3$ [14] (lone pair mechanism[15]), hexagonal $YMnO_3$ [16,17] (lattice improper ferroelectricity [DOI:10.1515/PSR.2019.0014]) or $TbMnO_3$ [18] (magnetic improper ferroelectricity [DOI:10.1515/PSR.2019.0016]). The numerous successes encountered by *first-principles* simulations established DFT as a powerful tool to design strategies for engineering magneto-electric multiferroic materials. Among all magneto-electric multiferroic materials, many studies considered ABO_3 perovskites, a well-known class of multifunctional materials of technological relevance. These compounds adopt an aristotype cubic structure where the A cations are located at the corner of the cell, the B cations are at its centre and are surrounded each by O_6 octahedra which form a corner sharing network. This structure is very attractive since it can accommodate various chemical elements on the A and B sites of the structure, including magnetic elements. According to the A-to-B cation size mismatch, measured through the Goldschmidt tolerance factor [19] $t = \frac{r_A + r_O}{\sqrt{2}(r_B + r_O)}$ where r is the ionic radius of the different ions, the structure can develop several lattice distortions such as O_6 rotations that in turn can alter the magnetic properties. Since the most popular ferroelectrics are perovskite oxides, it was straightforwardly used by theorists and experimentalists as a natural playground for engineering new properties and functionalities. Finally, developments of experimental techniques such as Pulse Laser Deposition (PLD) or Molecular Beam Epitaxy (MBE) allowing atomic-scale deposition of oxides as thin films, superlattices or nanostructures also favoured interest in oxide perovskites. In this article, we will therefore focus on this broad and promising family of compounds although, in practice, much more compounds can be multiferroic.

It is worth noticing that the choice of ABO_3 materials for engineering multiferroism was not *a priori* so judicious. Ferroelectricity and magnetism are expected to be mutually exclusive in ABO_3 materials, a fact formulated in terms of the "d^0" rule by Spaldin [20]. The rule relies on the fact

that ferroelectricity in prototypical ferroelectrics such as $BaTiO_3$ is related to *O 2p – B 3d* hybridization and requires empty *d* levels while magnetism requires partially filled *d*-states. The popular multiferroic material $BiFeO_3$ navigates around this rule with ferroelectricity held by the Bi cations at the A-site through a lone pair mechanism and magnetism carried by Fe cations at the B-site [14]. This has motivated the search of materials in which ferroelectricity and magnetism are driven by a different cation such as the double perovskite Bi_2FeCrO_6 [21–23]. Later in this chapter, we will see that in some cases magnetism and polar displacements can nevertheless be held by the same cation [24].

In this article, we first briefly discuss the key theoretical developments that made possible the prediction of novel multiferroic compounds using DFT simulations. We then highlight some strategies seeded by *first-principles* simulations that have been identified for engineering magneto-electric compounds. In fact, all these strategies typically rely on the basic concept of turning a non-polar magnet to a ferroelectric magnet. Namely, we will focus on the use of strain engineering, octahedra connectivity, lattice mode couplings, electronic or magnetic driven ferroelectrics (*i.e.* type II multiferroics) and interfacial systems based on an interface between a ferroelectric and a (anti-)ferromagnet.

I. Theoretical aspects

Density Functional Theory (DFT) is a powerful computational method aimed at solving the electronic problem. It is based on the Hohenberg and Kohn theorems [25] and the Kohn-Sham ansatz [26], that allows to find the ground state of the N many-body problem, associated with the wavefunction $|\psi(\vec{r})\rangle$ depending on 3N degrees of freedom, from the sole knowledge of the electronic density $\rho(\vec{r})$ that only depends on three spatial degrees of freedom. In its formulation, DFT is an exact theory. However, the exact form of the functional linking the energy to the density is unknown and must therefore be approximated. During the years, various approximate functionals have been developed which were successful for a wide variety of systems. Conceptualized in the sixties, DFT became a powerful computational tool during the eighties thanks to the advent of efficient supercomputers. Acknowledging this theoretical breakthrough, Walter Kohn was awarded the Nobel Prize in chemistry in 1998. We guide the reader to the textbook of R. Martin for a detailed and comprehensive description of DFT [27] as we will just provide the basic developments that have allowed studies of magneto-electric compounds with *first-principles* simulations. We describe below the standard methodologies used to model and compute ferroelectric, magnetic and magneto-electric properties.

1. Computing ferroelectric properties

In ferroelectrics, a fundamental quantity is the spontaneous electric polarization, defined in most textbooks as the dipole moment per unit cell. In truly periodic infinite solids as those considered by imposing Born-Von Karman boundary conditions, this quantity is however ill-defined (*i.e.* dependent on the arbitrary choice of the unit cell) which prevented practical computation of the polarisation for a long time. The breakthrough arose in 1992 with the modern theory of the polarization established by King-Smith and Vanderbilt as well as Resta who formulated the polarization as a Berry phase [28,29,30,31]. Independently, derivatives of the polarization such as the Born effective charges or piezoelectric constants are also accessible by

linear response using density functional perturbation theory [30–32]. More recently, methods have also been developed to deal with periodic solids under finite electric or displacement fields [33–35].

2. ***Modelling magnetic systems***

To study magneto-electric coupling, one obviously has to deal with magnetism. In this specific case, the DFT formulated by Kohn and Sham (Kohn-Sham DFT) can be easily extended to magnetic systems by treating separately spin up and spin down channels. One substitutes the scalar density $\rho(\vec{r})$ by a 2-by-2 $\overline{\overline{n}}(\vec{r})$ density matrix according to the following formula:

$$\overline{\overline{n}}(\vec{r}) \Longrightarrow \frac{1}{2}\begin{pmatrix} \rho(\vec{r}) + m_z(\vec{r}) & m_x(\vec{r}) - im_y(\vec{r}) \\ m_x(\vec{r}) + im_y(\vec{r}) & \rho(\vec{r}) - m_z(\vec{r}) \end{pmatrix} \quad \text{(eq.1)}$$

where $m(\vec{r})$ is the magnetic density. In addition to the scalar density $\rho(\vec{r})$ minimizing the energy, the spin-density $\overline{\overline{n}}(\vec{r})$ can also relax the magnetization both in magnitude and direction. At this stage, one must distinguish two cases: (i) the collinear approach reducing the spin polarized density to diagonal components, which is the most widely adopted methodology due to its more tractable computational effort (only $m_z(\vec{r})$ is considered as a scalar and thus spins can only relax in magnitude) and (ii) the non-collinear approach that considers the full 2x2 $\overline{\overline{n}}(\vec{r})$ density matrix that is computationally heavier, due to the presence of several local minima in the energy landscape as a function of relative spin directions (see section I.3 below).

By including the spin-orbit interaction, one fully considers the coupling between spin and orbital degrees of freedom and has access to spin canting and magnetocrystalline anisotropy. The spin-orbit coupling also allows to access to the orbital magnetization, which has been reached only very recently though a modern theory of magnetization [36–40], analogous to the Berry phase of the theory of polarization.

3. ***Approximation of exchange and correlation effects***

Although being in principle an exact theory of the ground state, DFT has some limitations in its practical implementation: it relies on an approximation of exchange and correlations effects, which often possess a spurious self-interaction problem (an electron is interacting with its own potential, potentially yielding undesired electron delocalization phenomena). The most common approximations to exchange and correlations are the Local Density Approximation (LDA) and Generalized Gradient Approximation (GGA, adding an additional term to LDA that depends on the density gradients) that have been successful in describing metals and band insulators. However, magneto-electric multiferroic materials involve magnetic cations, thus possessing partially filled *d* (or *f*) shells (*e.g.* for multiferroics based on *3d* elements for instance) and *de facto* a much more localized electronic structure. Standard approximations are usually not appropriate for studying such materials.

At the time of the revival of magneto-electric compounds, one had to use other methods to better treat electron-electron repulsion and cancel the spurious self-interaction term. The most widely adopted method is DFT+U, involving two empirical parameters U and J, corresponding to on-site Coulomb interactions and intra-site spin-exchange, respectively [41]. Both parameters are captured through a Hubbard-like model. We emphasize here that although the terminology '+U" is reminiscent of the Hubbard model, DFT is a single determinant theory with a static mean-field treatment of electron interactions, *i.e.* there are no dynamical correlation effects, and U is totally different to the interelectronic U parameter appearing in the Hubbard model. Typically, one usually fits these U and J parameters by adjusting their value in order to reach the best agreement with known experimental data, although methodologies exist to self-consistently evaluate these values [42,43]. However, the method is not always fully predictive and one might sometimes rescale the computed parameters [44]. Two different implementations of DFT+U exist, with U and J entering either as different parameters [45] or as a single effective U_{eff}=U-J parameter [46]. While the latter methodology is usually suited for collinear simulations, within few exceptions [47], both U and J parameters are important when dealing with non-collinear magnetic structures as J acts on the spin canting as demonstrated by Bousquet and Spaldin [48].

In the search of methods alleviating the use of empirical parameters, hybrid functionals also appeared as valuable methodologies. They combine LDA/GGA functionals with a part of exact Hartree-Fock exchange (thus forming "hybrid functionals") in order to better reproduce exchange and correlation effects and cancel the spurious self-interaction term. These functionals are usually providing a better description of structural aspects and band gaps over standard LDA and GGA functionals. The most famous hybrid functionals used for studying multiferroic materials are B3LYP [49] and HSE [50] and its updates. One must also highlight the B1WC functional that was developed to properly reproduce the properties of ferroelectric ABO_3 materials [51]. Although more computationally demanding than DFT+U methods, these hybrid functionals encountered many successes in modelling multiferroic materials [52–56]. Alternatively, they can be used as a starting point for extracting DFT+U parameters [54,57]. The very latest developments of meta-GGA functionals (adding an additional term depending on the second derivative of the density to GGA functionals), such as the SCAN functional [58], are producing insulating phases in most *3d* transition metal oxide perovskites and related compounds [59–61], and thus would be an invaluable method for studying multiferroism in the future.

We end this section by emphasizing that many alternative methods exist for studying multiferroic materials. For instance, Filippetti and Spaldin have developed a simplified Self-Interaction Correction method [62]. Alternatively, a post Hartree-Fock method[63] (Interaction Configuration) has been used to accurately compute the evolution of the magnetic exchange integrals as a function of an applied electric field in oxides with complex magnetic structures [64,65]. Finally, one can also invoke the most complex GW method including many body effects which was used to benchmark results on $BiFeO_3$ [52].

4. Computing the contribution to magneto-electric coupling

Now that we have exposed the basic methodologies and developments involved in the study of multiferroic compounds, we can focus more precisely on magneto-electric coupling. For the magneto-electric coupling, one usually refers to the magnetoelectric tensor which is a 2 by 2

matrix whose components (i,j) are given by the second derivative of the free energy F with respect to applied electric $\vec{E}$ and magnetic $\vec{H}$ fields:

$$\alpha_{i,j} = -\frac{1}{\Omega_0}\frac{\partial^2 F}{\partial E_i \partial H_j} = \frac{\partial P_i}{\partial H_j} = \frac{\partial M_j}{\partial E_i} \text{ (eq.2)}$$

where Ω_0 is the unit cell volume and P_i (M_i) is the polarization (magnetization) along the *i* axis. Within a Born Oppenheimer approximation, one can decompose the magneto-electric coupling into three contributions corresponding to electronic (α_{el}, pure electronic response at fixed atomic positions and lattice parameters), ionic (α_{ionic}, additional effect of atomic relaxation) and strain (α_{strain}, additional effect from lattice relaxation) parts. Let us remind here that for a magnetic system, the magnetization has two contributions originating from spin (labelled S) and orbital (labelled O), and thus the magneto-electric coupling is expected to have in total 6 contributions. To the best of our knowledge, the latest developments of DFT have calculated 5 out of 6 components of α [66–70] : only α^O_{strain} remains elusive.

Although revival of multiferroics began in the early 2000's, computation of the different components of the magneto-electric tensor only started in 2008. Again, boosted by experience with ferroelectric phenomena, Iñiguez proposed magnetic effective charges Z^m, analogous of Born effective charges Z^e, both given by the change of magnetization (polarization) with respect to an atomic displacement $\vec{u}$ [67]:

$$Z^m_{i,j} = \Omega_0 \frac{\partial M_i}{\partial u_j} \text{ (eq.3)}$$

$$Z^e_{i,j} = \Omega_0 \frac{\partial P_i}{\partial u_j} \text{ (eq.4).}$$

Using these quantities and by noting an analogy with the dielectric tensor, Iñiguez easily expressed the ionic part of the magnetoelectric coupling by the following formula:

$$\alpha^S_{ion,i,j} = \frac{1}{\Omega_0}\sum_{n=1}^{N_{IR}} \frac{Z^e_{n,i} Z^m_{n,j}}{K_n^2} \text{ (eq.5)}$$

where K_n are the eigenvalues of the force constant matrix and the sum runs over all infrared modes. K_n, $Z^e$and Z^m are directly accessible by DFT simulations and hence calculation of α^S_{ion} is rather straightforward. It was then extended to the orbital contribution in 2012 [70,71]. In the same

spirit, Wojdel and Iñiguez extended the formalism to the strain part of the magneto-electric coupling in 2009 [68]:

$$\alpha^{S}_{strain,i,j} = \frac{1}{\Omega_0}\sum_{m,n=1}^{3} e_{i,m}(C^{-1})_{mn}h_{j,n} \quad \text{(eq.6)}$$

where *e* and *h* are the piezoelectric and piezomagnetic tensors, respectively, and *C* is the elastic constant matrix.

In 2011, Bousquet *et al.* identified another pathway for computing the magneto-electric coefficients [66]: they proposed to evaluate the change of polarization under an applied magnetic field. The authors modelled the magnetic field $\vec{H}$ using a Zeeman term $\overline{\overline{\Delta}}V_{Zeeman}(\vec{r})$ that is added to the DFT scheme. It is represented by a very simple 2 by 2 matrix, reminiscent of the density matrix $\overline{\overline{n}}(\vec{r})$, and it takes the elegant expression:

$$\overline{\overline{\Delta}}V_{Zeeman}(\vec{r}) \Longrightarrow \frac{-g}{2}\mu_B\mu_0 \begin{pmatrix} H_z & H_x - iH_y \\ H_x + iH_y & -H_z \end{pmatrix} \quad \text{(eq.7)}.$$

By computing the change of polarization for different finite values of magnetic field, one can directly access the magneto-electric coupling components. Most notably, this technique has the advantage of giving access to the separate ionic and electronic parts of α^{S} (*i.e.* the electronic part is given at fixed lattice parameters and atomic positions while the ionic part is accessible once the structure is relaxed). While it was usually assumed that it is negligible in most cases, Bousquet *et al.* showed that α^{S}_{el} is about 25% of α^{S}_{ion} in the reference magnetoelectric material Cr_2O_3 [66], an antiferromagnetic (AFM) insulator below T_N=307 K adopting a centrosymmetric *R-3c* space group but whose magnetic structure allows a magnetoelectric effect. Going further, Ricci and Bousquet reported that α^{S}_{el} can be as large as α^{S}_{ion} in the troilite phase of FeS [72], which is attributed to the presence of a metal-insulator phase transition in this compound. In their paper, Ricci and Bousquet also reported that diagonal magnetoelectrics (compounds in which the magnetoelectric tensor reduces to diagonal components only) can be seen as being (electrically) polarized in opposite directions for each spin channel (up and down) such that the difference of the polarization contribution of each channel is non-zero (while the sum is exactly zero, FeS being non-polar). This can also be seen as the integration of the magnetic monopolar term (*e.g.* $\int_{\vec{r}} m(\vec{r}).\vec{r}\,.d\vec{r}$), also coined magnetoelectric monopolarization[73]. A full *first-principles* Berry

phase formulation and Wannier representation of the magnetoelectric monopole has been developed by Thöle, Fechner and Spaldin[74], which paves the road to systematically compute this original property of magnetoelectric crystals. Finally, the strategy developed by Bousquet and Spaldin was employed in 2016 by Tillack, Yates and Radaelli to disentangle the different contributions – cycloidal, longitudinal and chiral terms -- to the magnetoelectric tensor in Cr_2O_3 in the low-field and spin-flop phases[75].

Later on, the computation of magnetic properties as a function of an applied electric field, thanks to the emergence of the modern theory of magnetization, enabled access to the orbital part to the magneto-electric coupling. Again, using Cr_2O_3 as the prototypical example, Malashevich and co-workers showed that the orbital contribution to α (both electronic and ionic parts) are smaller than the spin contribution[71]. However, Scaramucci *et al.* found distinct results in $LiFePO_4$ with rather similar spin and orbital contributions to α_{ion}[70]. So far, and to the best of our knowledge, the orbital contribution to the strain part of the magneto-electric coupling has not been computed.

Similarly to the monopolarization in "diagonal magnetoelectrics", another exotic property can be associated to non-diagonal magnetoelectrics: the bulk magnetic toroidal moment[73]. Identically to the electric toroidal moment, the magnetic (or spin) toroidal moment can be described by $\sum_i \vec{r}_i \,.\, \vec{m}_i$, where $\vec{m}_i$ is the magnetic moment at position $\vec{r}_i$. This magnetic toroidal moment is directly associated to the antisymmetric part of the magnetoelectric tensor and it breaks both space and time reversal symmetries together. A new primary ferroic order (on the top of the ferroelectric one, which breaks the space inversion only, of the ferromagnetic one, which breaks the time reversal only and of the ferroelastic one, which is invariant under both space and time reversal), *i.e.* ferrotoroidic, could be defined where the toroidal moment would be an independent order parameter[76,77]. Recently, Gao, Vanderbilt and Xiao have developed a microscopic theory of spin toroidization for periodic crystal[78] but its implementation in a DFT code is still lacking.

5. Accessing finite temperature properties.

Finally, DFT simulations are performed at 0 K. Complementary methods have been involved in order to alleviate this restriction imposed by DFT simulations. Using Monte-Carlo simulations combined with DFT calculations, Mostovoy *et al.* have considered the spin fluctuations coming from thermal effects [79]. They showed that these exchange-striction effects can break the inversion centre in Cr_2O_3 (that is otherwise centrosymmetric) and induce a polarization, resulting in a magneto-electric effect in the material. Additionally, they demonstrated that the contribution of the spin-orbit interaction to α is one order of magnitude smaller than the exchange-striction effects. These results are supported by quantum chemistry calculations of Varignon *et al.* on $YMnO_3$ that showed that the modification of magnetic exchange integrals under an applied electric field (*i.e.* somehow indicative of the strength of the magneto-electric coupling) are mainly governed by striction effects rather than by the spin-orbit interaction [65].

Finally, *second-principles* methods are constantly on the rise to grant access to finite temperature properties. For instance, effective Hamiltonians of Bellaiche and co-workers gave access to the magneto-electric coefficients and to the origin of the spin-spiral of $BiFeO_3$ [80,81]. Such a work relies on the effective Hamiltonian approach, initially developed for ferroelectrics during the '90s[82,83]. Further generalization of effective Hamiltonians has been proposed in order to treat explicitly all structural degrees of freedom from the construction of first-principles based effective atomic potentials[84], as implemented in SCALE-UP [www.secondprinciples.unican.es/spdft] and MULTIBINIT [www.abinit.org] softwares. More recently, the method has even been extended in order to reintroduce electronic degrees of freedom[85] and perform second-principles simulations at finite temperature while considering explicitly lattice and electron degrees of freedom. This opens new perspectives for the modelling of magneto-electric multiferroics at the mesoscale and finite temperatures.

II. Strain engineering

1. *Inducing ferroelectricity in magnets*

The advent of experimental growth techniques allowing atomically-controlled deposition of epitaxial oxides thin films has enabled promising pathways for engineering new physics and phenomena with ABO_3 oxides. In 2004, the identification of room-temperature ferroelectricity under moderate tensile epitaxial strain in $SrTiO_3$, an otherwise quantum paraelectric material in bulk, offered promising perspectives for multiferroism [86]. It became straightforward to use such a strategy to induce ferroelectricity in magnetic materials.

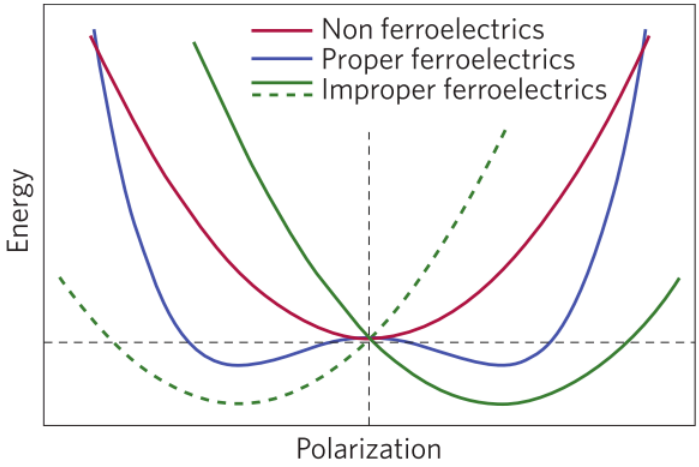

Figure 1: Energy potential as a function of a polar displacement. Figure extracted from Ref.[87].

This strategy is universal and relies on the coupling between the ferroelectric polarization P and the homogeneous strain η. In the high-symmetry cubic cell of ABO_3 compounds, the lowest-order $P-\eta$ coupling term to the free energy takes the form $g\eta P^2$, so that we can write:

$$F(P,\eta) \propto (a+g\eta)P^2 + bP^4 + \varsigma\eta^2 \propto a_{eff}P^2 + bP^4 + \varsigma\eta^2 \quad \text{(eq.8)}$$

where *a, b, c,* ς and *g* are coefficients. For non-polar compounds in bulk (*i.e.* $\eta = 0$), the coefficient a is positive, and the energy as a function of a polar displacement P is characterized by a single well energy potential whose minimum is located at P=0 (red curve of Figure 1). For a "proper ferroelectric" in bulk, the coefficient a is negative and the system is then characterized

by a double well potential whose minimum is now located at $P \neq 0$ (*i.e.* $+P_S$ and $-P_S$) (blue curve in Figure 1) [88]. For a non-polar material in thin film form, the effect of the epitaxial strain η is to renormalize the coefficient of equation 8 into a_{eff}. For η sufficiently large and with appropriate sign, a_{eff} can become negative and produce a ferroelectric behaviour. Thus, turning a non-polar compound to a ferroelectric is *a priori* feasible for any material *via* strain engineering whatever the sign of the coefficient *g* is: if *g*>0, one would use compressive strain (*i.e.* η<0) and if *g*<0, one involves tensile strain (*i.e.* η>0). However, the strength of the $P - \eta$ coupling is different for each material and not necessarily large so that being already at the verge of a ferroelectric transition (*i.e.* having a polar phonon mode at relatively low frequency) is often a prerequisite to destabilize the system at experimentally achievable epitaxial strains.

This powerful strategy encountered many successes and most notably, it has been employed to demonstrate that magnetism and ferroelectricity are not mutually exclusive but can coexist in $CaMnO_3$ [24]. In bulk, $CaMnO_3$ is a G-type AFM insulator adopting a *Pnma* symmetry characterized by the usual $a^-b^+a^-$ oxygen cage rotations in Glazer's notation [89] (see Figure 2.d for sketched of magnetic orders). However, on the basis of *first-principles* simulations, Bhattacharjee, Bousquet and Ghosez have identified in the cubic phase that $CaMnO_3$ does exhibit both weak ferroelectric and large oxygen cage rotation imaginary phonon frequencies ω – one recalls here that the curvature of the energy *E* is proportional to ω^2. While the ferroelectric mode instability is suppressed by the rotations in bulk, they proposed that appropriate strain engineering can make $CaMnO_3$ ferroelectric. This scenario was verified experimentally in 2012 by applying a 2.3% tensile strain to the material [90]. This result attracted some attention since it was showing for the first time that both ferroelectricity and magnetism can be held by the B site cations[24], thus breaking somewhere the "d^0" rule.

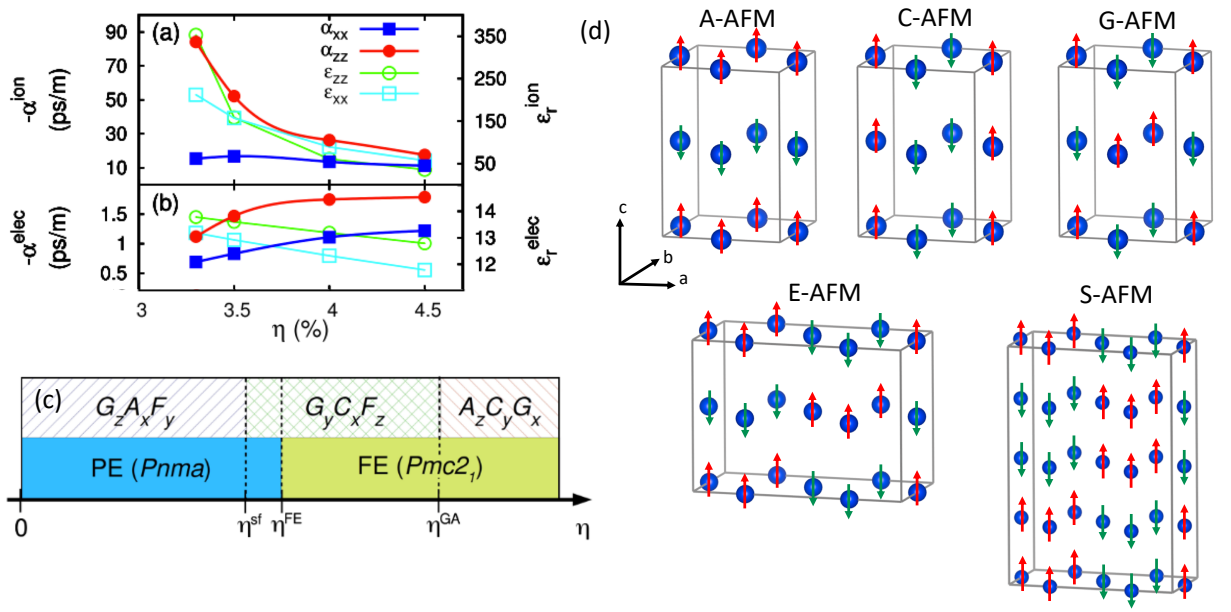

Figure 2: Multiferroic properties of $CaMnO_3$ under strain engineering. xx (squares) and zz (circles) components of the magneto-electric (filled symbols) and dielectric (open symbols) constant versus the epitaxial strain for ionic (a) and electronic (b) contributions. (c) Structural, ferroelectric and magnetic properties of $CaMnO_3$ versus epitaxial strain. η^{sf} = 2.6 % is the strain value needed for inducing a spin-flop transition, η^{FE}=3.2 % corresponds to the strain required for the non-polar - ferroelectric transition and at η^{GA}= 4.6%, the magnetic order switches from a G-type to a A-type. (d) Sketched of magnetic orders appearing in orthorhombic perovskites. The orthorhombic structure corresponds to a $(\sqrt{2}a_c, \sqrt{2}a_c, 2a_c)$ cubic cell where a_c is the cubic cell lattice parameter. Panels (a), (b) and (c) are adapted from Ref.[91].

Being ferroelectric and magnetic does not necessarily imply that there is a large magneto-electric effect in the material. The existence of a linear magneto-electric effect in strained $CaMnO_3$ was verified by Bousquet and Spaldin in 2011 [91]. In any material adopting a *Pnma* symmetry with a G-type AFM order, a small canting of spins is allowed thus permitting weak ferromagnetism along the *z* axis (see Ref. [92] for a detailed description of non-collinear magnetism). Nevertheless, the inversion centre existing in the *Pnma* symmetry forbids any magneto-electric effect [93]. By using strain engineering, Bousquet and Spaldin have shown that $CaMnO_3$ adopts a *Pmc2₁* ferroelectric phase at 3.2 % of tensile epitaxial strain (see Figure 2.c). Although the easy axis rotates with respect to the *Pnma* symmetry at 2.6 % of strain, a linear magneto-electric effect is allowed with ionic and electronic components larger than that exhibited by Cr_2O_3 (see Figures 2.a and 2.b) [91]. For tensile strains larger than 4.6%, another

magnetic phase transition from a G-AFM to a A-AFM order at constant structural symmetry occurs but a linear magneto-electric effect is not anymore allowed (Figure 2.c and 2.d). This symmetry analysis is totally general and may apply to any material adopting a *Pnma* symmetry, which is the most common symmetry adopted by ABO_3 perovskites. A recent group theory analysis led by Senn and Bristowe has enumerated the possible couplings between polarization and magnetism in ABO_3 perovskite oxides[94].

In addition to unlocking ferroelectricity in some otherwise non-polar materials in bulk, strain engineering can also unveil unexpected ferroelectric phases in perovskites. For instance, it has led to a rich ferroelectric phase diagram as a function of the applied epitaxial strain in $BiFeO_3$, including a super-tetragonal phase for highly compressive strain [95,96] (T phase briefly discussed in Section II.3, see chapter on $BiFeO_3$ by Bibes *et al.* for further details). Another "super-ferroelectric" phase is also achieved under large tensile in ABO_3 ferroelectrics, such as $PbTiO_3$ [97,98], or otherwise non-polar compounds in bulk such as $SrTiO_3$ and $BaMnO_3$ [99]. Strain can also be applied to superlattices such as $(SrCoO_3)_1/(SrTiO_3)_1$ [100] or $(PbTiO_3)_1/(SrTiO_3)_1$ [101] for engineering various ferroelectric phases. Finally, strain engineering is not restricted to ABO_3 materials. For instance, Bousquet and co-workers have proposed that it can yield ferroelectricity in simple magnetic binary oxides like EuO [102] or multiferroicity in fluorite ABF_3 compounds [103,104].

2. ***Inducing magnetism in ferroelectrics***

Additionally to induce ferroelectricity, Spaldin and co-workers have unveiled that strain also favours the formation of oxygen vacancies in oxides films such as in $CaMnO_3$ [105,106] (the inverse effect was also shown theoretically and experimentally in $PrVO_3$ thin films [107]). This additional lever offers nice perspectives for unlocking new functionalities in oxides and for engineering multiferroism [108]. For instance, on the basis of DFT calculations, Xu *et al.* have shown that strain can favour the appearance of defects in the ferroelectric non-magnetic $PbTiO_3$, giving rise to magnetism and thus to multiferroism [109].

3. ***Structural softness***

Equations 5 and 6 proposed by Iñiguez and co-workers clearly suggest a route to design compounds with large magneto-electric effects: vanishingly small values of K_n or C will produce diverging behaviours for α [68] and thus large magneto-electric response. This is coined as a "structural softness". Since the dielectric constant ε_{ion} also diverges, positioning the material close to a ferroelectric phase transition may result in the enhancement of α. Iñiguez and Wojdel proposed to use the rhombohedral (R) and tetragonal (T) polymorphs of $BiFeO_3$ as a proof of concept. As a function of the applied compressive epitaxial strain, they found that the transition from R to T phase occurs at 4.4 %. Nevertheless, the authors observed a strong enhancement of the magneto-electric coefficient for the R phase at 6% strain (see Figure 3), although not the ground state at this strain level, which is ascribed to a phonon with a vanishingly small force-constant.

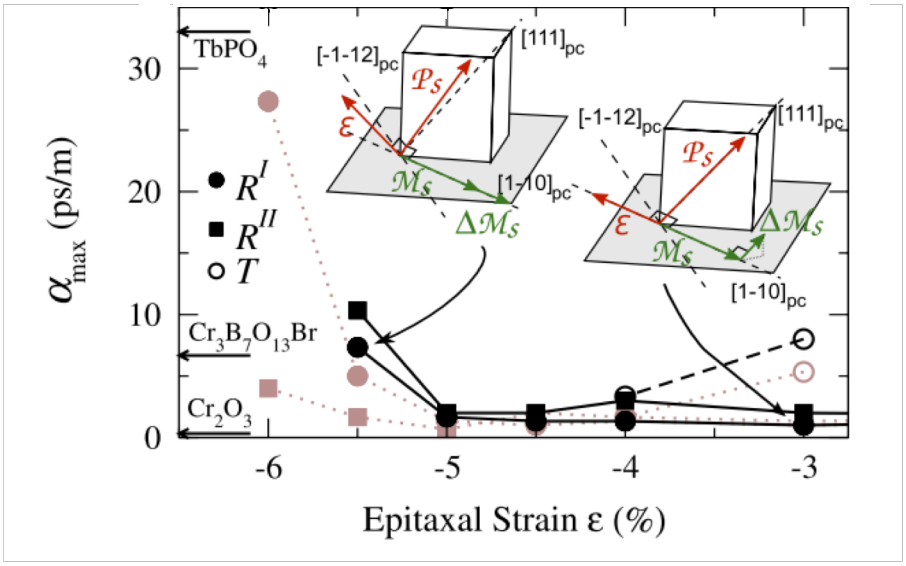

Figure 3: Magneto-electric response of the rhombohedral R (filled symbols) and tetragonal T (open symbols) phases as a function of the epitaxial strain. Figure extracted from Ref.[110].

4. ***Phase competitions through spin-lattice coupling***

In magnetic materials, exchange interactions are directly affected by changes of structural aspects such as modifications of B-O bond lengths and/or B-O-B bond angles. Consequently, they are sensitive to the optical phonon modes appearing at the zone centre. The frequency ω associated with these phonon modes are in turn sensitive to spin orders. This phenomenon is coined as "spin-lattice coupling" and the frequency ω can be written as [111–113]:

$$\omega \propto \omega_{PM} + \gamma\langle \vec{S}_i . \vec{S}_j \rangle \quad \text{(eq.9)}$$

where ω_{PM} is the frequency in the spin-disordered paramagnetic (PM) phase, $\langle \vec{S}_i . \vec{S}_j \rangle$ is the nearest neighbour spin-spin correlation function in the cell and γ is the spin-lattice constant. We can simply express the free energy as a function of the polar P and the ferromagnetic L (antiferromagnetic M) order parameters:

$$F(P, L) \propto +\gamma' P^2 L^2 \quad \text{(eq.10)}$$

$$F(P, M) \propto -\gamma P^2 M^2 \quad \text{(eq.11)}$$

It appears that, similarly to strain in equation 8, the magnetic order can produce a significant renormalization of a ferroelectric phonon frequency. In this case however, the coupling is bi-quadratic (see also Section IV.3 for a similar example of lattice mode coupling) so that induce polarization will mandatorily require a positive coefficient. In such a case, starting from a non-polar material, a sufficiently large γ can produce a sizable renormalization of the zone-centre mode frequencies and induce ferroelectricity in the material.

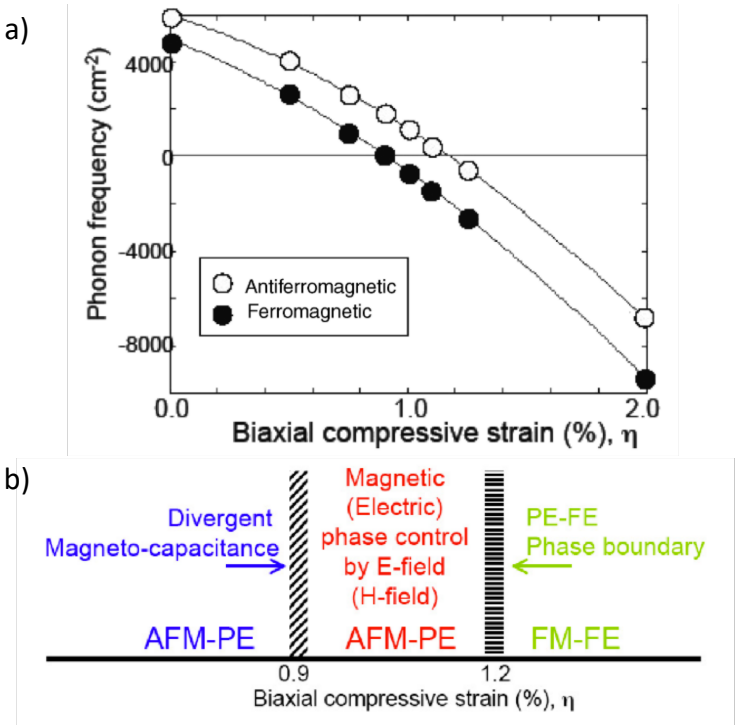

Figure 4: (a) Phonon frequency of a ferroelectric mode as a function of the epitaxial strain for a ferromagnetic (filled circles) and an antiferromagnetic (open symbols). (b) Phase diagram of $EuTiO_3$ as a function of the epitaxial strain. PE and FM stand for paraelectric and ferromagnetic, respectively. Figures extracted from Ref.[113].

This mechanism can be coupled to strain engineering to bring the material close to a phase competition between two magnetic states. This is the strategy employed by Fennie and Rabe in $EuTiO_3$, an antiferromagnetic material adopting a non-polar cubic structure at all temperatures [113]. As a function of the biaxial compressive strain applied to the material, the authors observed that the critical value to destabilize a ferroelectric phonon mode is smaller for a ferromagnetic state than for the antiferromagnetic configuration (see Figure 4.a). It follows that there is a narrow region between 0.9 % and 1.2 % of biaxial strain where the material possesses competing ferroelectric-ferromagnetic (FE-FM) and antiferromagnetic-paraelectric (AFM-PE) (see Figure 4.b). Locating the material in this narrow compressive strain region offers a control of magnetic properties with an electric field: applying a magnetic field aligns the spins ferromagnetically (FM), and thus the material becomes a ferroelectric. Conversely, applying an electric field will force a ferromagnetic alignment of the spins. We emphasize that the ground state of $EuTiO_3$ remains AFM-PE until 1.2 % of biaxial strain (Figure 4.b). The existence of the FE-FM phase at larger strain

values was confirmed experimentally [114] although a tensile strain was involved -- we highlight that the effect of the epitaxial strain is similar for compressive and tensile strain, the polar axis is just rotated by 90° between the two strain states.

Although a nice proof of concept, the low Néel temperature of $EuTiO_3$ ($T_N \propto 5.5$ K) hinders practical use of the material. Going from materials involving *4f* elements to materials implying *3d* elements is a good alternative. Lee and Rabe have proposed that $SrMnO_3$, an antiferromagnetic material with a T_N around 250 K in bulk, exhibits a large spin-phonon coupling and adopts a ferromagnetic-ferroelectric ground state at large epitaxial strain [115]. Large spin-phonon coupling was also observed in materials with magnetism carried by both *4f* and *3d* elements [116]. Finally, strong coupling between magnetism and lattice degrees of freedom is not restricted to ABO_3 materials with a perovskite structure. It has been also observed in hexagonal materials such as $YMnO_3$ [117,118] or in MnF_2[119].

III. Oxide interfaces

When computing the phonon dispersion curves of most ABO_3 compounds in their ideal high symmetry cubic phase, one often identifies several unstable phonon frequencies associated with polar zone-centre modes. This is the case, for instance, in $CaTiO_3$ (see Figure 5.a) [120]. However, one observes other unstable phonon modes associated with oxygen cage rotations, also called antiferrodistortive motions, located at the M and R points of the Brillouin zone – $a^0b^+a^0$ and $a^-b^0c^-$ rotations in Glazer's notation [89], respectively. They usually produce larger energy gains than the unstable ferroelectric modes and, when appearing, in turn usually compete with and suppress the ferroelectric instability [120] (through a bi-quadratic energy coupling of the form $F \propto g\, \emptyset^2 \,.\, P^2$ with g>0 and ∅ a rotation). Weakening the oxygen rotations should reversibly favour and reintroduce the ferroelectric instability. This physical behaviour was highlighted by Kim *et al.* in $NdNiO_3$, adopting in bulk at low temperatures an antiferromagnetic and non-polar insulating structure characterized by oxygen cage rotations [121]. In thin films, as a function of the rotation mode amplitude (labelled tilt angle in Figure 5.b), the authors show that the two ferroelectric

phonons modes initially stable in the "bulk" (*e.g.* for a tilt angle of approximately 11°) acquire an imaginary frequency upon decreasing the rotations amplitude (Figure 5.b) – we recall that curvature of $E \propto \omega^2$. Consequently, by reducing the amplitude of rotations of O_6 motions, the material can become ferroelectric.

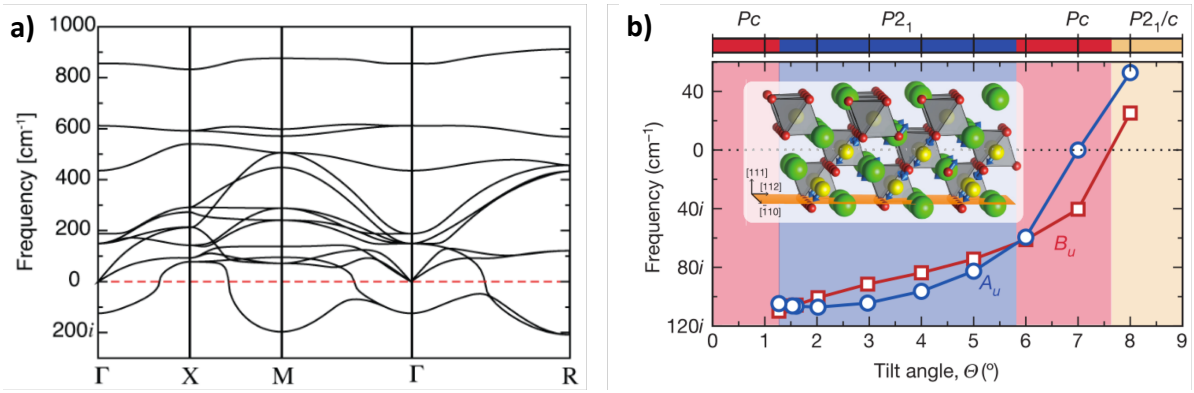

Figure 5: (a) Phonon dispersion curve of $CaTiO_3$ in its high symmetry Pm-3m cubic cell. Figure extracted from Ref.[120]*. (b) Evolution of the frequency associated with two ferroelectric phonon modes as a function of the rotation amplitude in $NdNiO_3$. Figure extracted from Ref.*[121]*.*

To verify this experimentally, a practical strategy consists in interfacing the material of interest with another perovskite that possesses weaker O_6 groups rotations. At the interface between the two compounds, O positions are locked and the amplitude of antiferrodistortive motions in the material of interest is decreased. In order to maximize the interfacial effect, (111)-oriented films are preferred since three O positions are locked at the interface instead of 1 and 2 for (001) and (110) oriented films respectively (see Figure 6.a). This is the strategy employed by Kim *et al.*: they interfaced $NdNiO_3$ with $LaAlO_3$, a band insulator with small O_6 rotations. They observe that AFD motions are strongly altered near the interface (see Figure 6.b). Second Harmonic Generation measurements then revealed the existence of polar domains. Combined with its AFM state at low temperature, $NdNiO_3$ is a multiferroic compound. Yet, no report of a magneto-electric effect has been reported nor measured to the best of our knowledge.

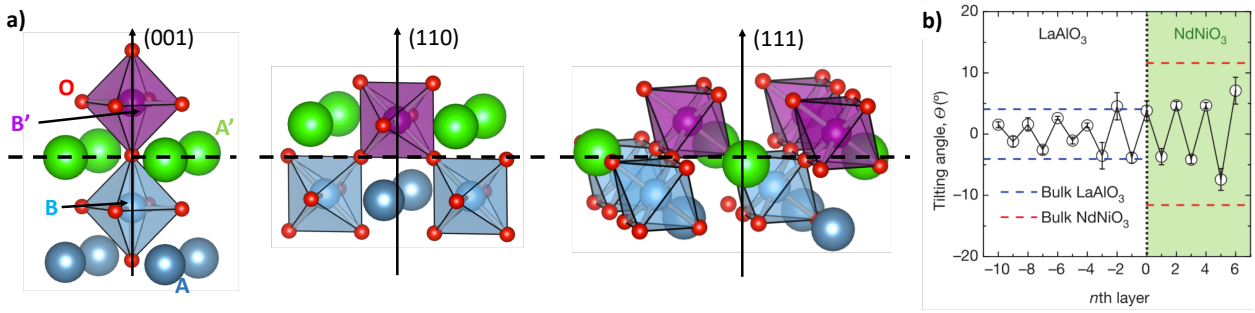

Figure 6: (a) Octahedra connectivity at oxide interfaces according to the different growth orientations. (b) Evolution of the rotation angle near the interface between (111) oriented $LaAlO_3/NdNiO_3$ interfaces. Bulk angles correspond to the dashed lines. This figure is extracted from Ref.[121].

Since most ABO_3 perovskites adopt the orthorhombic *Pnma* symmetry -- or lower symmetry -- characterized by the usual octahedral rotations, growth of oxide interfaces is an appealing strategy to design multiferroic compounds with potentially large magneto-electric effects.

IV. Lattice mode couplings

1. *The concept of lattice improper ferroelectricity*

So far, we have discussed strategies to induce ferroelectricity by destabilizing an otherwise "stable polar phonon", *i.e.* acting directly on the energy curvature at the origin (from red to blue curve in Figure 1). Nevertheless, some materials are ferroelectric despite the fact that the curvature of the ferroelectric mode remains positive at the origin (from red to green curve in Figure 1).

$YMnO_3$ is a prototypical example of that type. It is a multiferroic compound that adopts a hexagonal symmetry instead of the usual cubic variants due its very small tolerance factor. At 1258 K, this material undergoes a structural phase transition from a centrosymmetric *$P6_3/mmc$* phase to a polar *$P6_3cm$* ground state, involving a unit cell tripling. Fennie and Rabe have evidenced that there isn't any polar instability in the centrosymmetric *$P6_3/mmc$* phase [17] (see Figure 7 upper panel). Instead, they identified that a non-polar K_3 mode at the zone boundary is unstable in the high-symmetry phase, further being responsible of the phase transition and of the unit cell tripling. Interestingly, they identified the following coupling term between the polarization P and the non-polar K_3 mode in the free energy:

$$F \propto c.Q_{K_3}^3.P \quad \text{(eq.12)}$$

where *Q* is the amplitude of distortion associated with the K_3 mode and *c* is a coefficient. Since this term is linear in P, at the structural phase transition, the condensation of the K_3 mode will progressively shift the single well associated with the polar mode to lower energy and finite *P* amplitude (see Figure 7). The polarization is therefore not intrinsically unstable but appears to be a slave of the primary non-polar order parameter. Materials exhibiting such a behaviour are coined as "improper ferroelectrics" (green curves in Figure 1). Improper ferroelectrics have physical properties distinct from those of proper ferroelectrics: (i) switching the polarization will necessarily require the reversal of the primary non-polar distortion (green dashed line in Figure1); (ii) they do not show divergence of their dielectric properties at the phase transition [122] (*i.e.* they

don't obey the Curie-Weiss law since the polar mode does not soften) and (iii) they are less sensitive to depolarizing field issues [11,123,124].

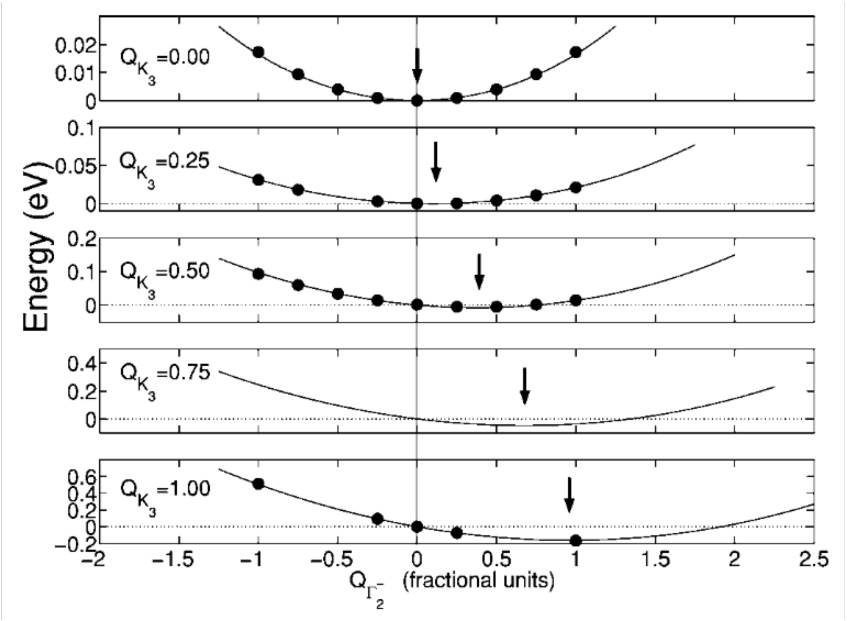

Figure 7: Energy potential as a function of the polar distortion at fixed amplitude of the K_3 mode in $YMnO_3$. This figure is extracted from Ref.[17].

After this mechanism was revealed in $YMnO_3$, Varignon and Ghosez proposed that $BaMnO_3$ in its 2H hexagonal polymorph also exhibits improper ferroelectricity despite totally different atomic structure and formal oxidation states of cations with respect to $YMnO_3$ [56]. The unit cell tripling in 2H-$BaMnO_3$ was observed experimentally by the group of Kamba but the improper nature of the polarization couldn't be confirmed nor implied [125]. In 2017, Xu *et al.* have proposed general strategies to design new improper ferroelectrics using ABO_3 perovskites as a platform[94]. Most notably, they identified that the otherwise centrosymmetric *R-3c* structure (hexagonal symmetry adopted by $LaAlO_3$ for instance) can exhibit improper ferroelectricity by substituting half of the B site cations using $(ABO_3)_2/(AB'O_3)_2$ superlattices [126]. It results in a polar C_2 symmetry possessing a linear coupling between P and the amplitude Q of a rotation of the form $F \propto P.Q$ in the free energy expansion F starting from a high symmetry *R-3m* phase. This mechanism is identical to that previously established by Young and Rondinelli in 2014 in (111)-oriented $(RAlO_3)_1/((PrAlO_3)_1$ superlattices with R=La or Ce, *i.e.* superlattices based on non-polar

materials adopting a *R-3c* structure [127]. Finally, ABO_3 improper ferroelectrics with a coupling between P and another non-polar motion remains scarce and to the best of our knowledge, these ABO_3 improper ferroelectrics have so far only involved hexagonal systems.

2. ***Hybrid improper ferroelectricity***

As we already stated in section III, the oxygen rotations appearing in *Pnma* phases – or lower symmetries – are usually annihilating ferroelectric instabilities identified in many perovskites. To be more precise, Benedek and Fennie have demonstrated that, beyond rotation themselves, the additional presence of A site cation anti-polar displacements minimizing A-O repulsion further suppresses the ferroelectric instability [120]. These A-site anti-polar displacements, associated to the X point of the Brillouin zone and labelled A_X (see Figure 8.a) are usually not intrinsically unstable in the cubic phase but are boosted by the joint presence of out-of-phase $a^-b^0c^-$ (labelled $\emptyset_1$) and in-phase $a^0b^+c^0$ (labelled $\emptyset_2$) rotations in Glazer's notations [89] thanks to the following term in the free energy expansion:

$$F \propto e\emptyset_1\emptyset_2 A_X \quad \text{(eq.13)}.$$

These anti-polar motions create locally on each plane a net polarization that is nonetheless cancelled by the very same motion pointing in the opposite direction on the consecutive plane along the *z* axis, resulting in no net polarization in the material (Figure 8.a). In 2012, Rondinelli and Fennie proposed to substitute half of the A site cations by using $(ABO_3)_1/(A'BO_3)_1$ (001)-oriented superlattices [128] : since A and A' cations do not have similar masses and charges, they produce different local polarizations on consecutive planes along the *z* axis (see Figure 8.b). Consequently, it results in a net polarization in the material that is coupled to the two rotations by the following unusual trilinear term in the free energy expansion

$$F \propto e'\emptyset_1\emptyset_2 P \quad \text{(eq.14)}.$$

Since this term is linear in P, the joint condensation of $\emptyset_1 \text{and } \emptyset_2$ modes will progressively shift the single well associated with the polar mode and produce a spontaneous polarization, similarly to what was previously discussed for improper ferroelectrics (Eq. 12). This time, however, the joint action of two distinct modes is required to drive the polarization.

The appearance of a spontaneous polarization through such a trilinear term was first discovered by Bousquet *et al.* [129] in 2008 on $SrTiO_3/PbTiO_3$ superlattices – while involving slightly different rotation patterns of octahedra and orientation of the polarization – and is nowadays referred to as "hybrid improper ferroelectricity" (HIF) [130].

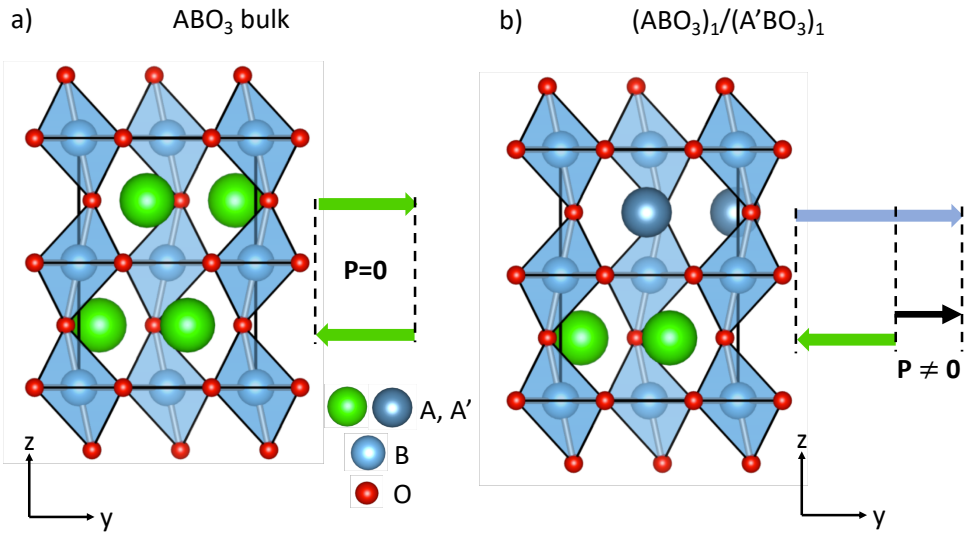

Figure 8: Illustration of anti-polar displacements in bulk ABO_3 compounds (a) and ferri-like polar distortions in $(ABO_3)_1/(A'BO_3)_1$ superlattices (b).

HIF is not restricted to 1/1 superlattices and to octahedral rotations and it has since 2008 been extended to (i) 2/2 superlattices involving identical A cations but two different B cations such as $(YFeO_3)_2/(YTiO_3)_2$ superlattices [131]; (ii) thin film forms of oxides such as highly strained $BiFeO_3$, $PbTiO_3$, $SrTiO_3$ or $CaTiO_3$ [98,99,132]; (iii) hybrid organic-metal organic perovskites [133,134]; (iv) double perovskite systems such as $NaLaMnWO_6$ [135] or $RLaMnNiO_6$ [136] (R=Lu-La, Y); (v) Jahn-Teller motions or anti-polar motions [98,99,132–134,137–140] and (vi) other types of layered perovskites such as Ruddlesden-Popper [130,141,142], Aurivilius[143] or Dion-Jacobson [144,145] (we invite the reader to Ref.[146] for a detailed discussions of these materials).

Hybrid improper ferroelectricity is nowadays a well-established strategy to design multiferroic materials since many (magnetic) perovskites adopt the required tilt-pattern of O_6 groups: one can cite layered titanates $(A^{2+}TiO3)_1/(R^{3+}TiO3)_1$ (A and R are an alkaline-earth and a rare-earth element, respectively) that would form ideal multiferroics with coexisting

ferromagnetism and ferroelectricity [57] or double layered $(R_2NiMnO_6)_1/(La_2NiMnO_6)_1$ systems that are predicted to be near-room temperature multiferroic compounds [136]. Although *a priori* a theoretical concept, hybrid improper ferroelectricity has been observed experimentally in $(Ca,Sr)_3Ti_2O_7$ and $(Ca_ySr_{1-y})_{1.15}Tb_{1.85}Fe_2O_7$, Ruddlesden-Popper compounds (naturally layered perovskites) [147,148].

Several theoretical and experimental efforts are still devoted to understand HIF in perovskites and related materials and to rationalize rules maximizing the polarization [57,101,152–156,126,128,141,142,146,149–151]. One key point is to understand the phase transition of these materials: are there single or multiple phases transitions or is it an avalanche effect with all modes appearing at once [152]? Another key aspect is the polarization reversal mechanism: since the trilinear term (eq. 14) imposes to switch one of the non-polar distortion together with the polarization to keep the energy invariant, the switching path is not trivial and should be better clarified. Even, the ability to reverse the polarization in hybrid improper ferroelectrics is questionable [130,157–159].

In addition to producing ferroelectricity in otherwise non-polar materials, HIF is a promising "knob" to tune large magneto-electric responses as suggested by Bousquet *et al.* in their seminal work of 2008 [129]. As highlighted above, in such systems, the reversal of the polarization P necessarily requires the switching of a non-polar lattice distortions (either $\emptyset_1$ or $\emptyset_2$) that can be coupled to the magnetism. Fennie and Benedek realized this in $Ca_3Mn_2O_7$ [130]: using *first-principles* calculations, they demonstrated that the two O_6 group rotations not only induce the polarization but that they also produce weak ferromagnetism and a linear magneto-electric effect. Thus, switching the polarization can reverse the magnetization by the reversal of one rotational mode. A similar mechanism has been exploited by Zanolli *et al.* in (001)-oriented $(BiFeO_3)_1/(LaFeO_3)_1$ superlattices [159]. However, we emphasize again that the switching path remains a fundamental aspect for these materials[157].

Since the initial exploitation of rotational modes, other works proposed to harness other lattice distortions intimately coupled to the electronic structure or to magnetism. A key lattice

distortion behind many properties of perovskites is the Jahn-Teller motion: it can lift orbital-degeneracies of ions and affect the magnetic-interactions through strongly entangled spin-orbital degrees of freedom [160]. In 2015, Varignon, Bristowe, Bousquet and Ghosez exploited the two competing Jahn-Teller (JT) motions, each forcing a dedicated magnetic order, of rare-earth vanadates to unveil a ferroelectric control of magnetism in (001)-oriented 1/1 superlattices [137] *via* an electrical control of the JT modes. Although no effect on magnetic orderings was discussed, some of these authors also proposed a ferroelectric control of JT distortions in highly strained oxide perovskites [99].

3. ***Embedding ferroelectricity and octahedra rotation in a single phonon mode***

While the switching pathway is the main drawback of improper and hybrid improper ferroelectrics to have the polarization/magnetization coupling in perovskites, Garcia-Castro *et al.* reported that a solution to this problem is to entangle octahedra rotations and ferroelectric polarization in a single soft phonon mode[161]. They reported such a possibility in $BaCuF_4$, which is polar directly below its melting temperature (1000 K) and is a canted antiferromagnetic below its Néel temperature (T_N=275 K) with weak ferromagnetism, thus making $BaCuF_4$ multiferroic. In their DFT calculations, Garcia-Castro *et al.* showed that reversing the polarization always reverses the weak ferromagnetic moment in $BaCuF_4$. This systematic flipping of the magnetization with the polarization is attributed to the presence of both polar distortions and octahedra rotations in a single zone center polar unstable mode of the high symmetry phase *Cmcm*. This means that polarization and octahedra rotations are not coming from the coupling of two different phonon modes but are instead entangled within a single eigenvector, which also means that reversing this single eigenvector necessarily drive the reversing of all the associated distortions (*e.g.* polar displacements plus octahedra rotations). In such situation the coupling between polarization and octahedra rotation is thus ideal and since the weak ferromagnetism is driven by the octahedra rotation, there is also a perfect reversing of the weak ferromagnetism with the polarization. This case thus avoids the drawback of improper ferroelectricity where there is no guaranty to switch the octahedra rotation driving weak ferromagnetism with the polarization. This result thus opens

a new direction for seeking new multiferroism in perovskites related materials where the polarization is directly coupled to the weak ferromagnetism.

4. Triggered-like ferroelectrics

While most perovskites adopt an orthorhombic *Pnma* cell with $a^-b^+a^-$ oxygen cage rotations, some compounds crystallize in a ferroelectric *R3c* structure characterized by $a^-a^-a^-$ oxygen cage rotations due to a tolerance factor largely deviating from 1. This is the case of $ZnSnO_3$ that, surprisingly, exhibits an additional ferroelectric distortion that cannot origin from a lone pair mechanism (Zn^{2+} cations do not have a lone pair, *e.g.* unlike $BiFeO_3$) or a "d^0" rule (Sn^{4+} cations do not possess *d* electrons in conduction band, *e.g.* unlike $BaTiO_3$).

In cubic perovskites, oxygen rotations and polarization can only couple together at even orders yielding therefore the following terms in the energy expansion:

$$F \propto (a + b\emptyset^2 + c\emptyset^4 + \cdots)P^2 \propto a_{eff}P^2 \quad \text{(eq.15)}$$

As previously discussed (see Section III), oxygen rotations and polarization typically compete at the bi-quadratic level (*i.e.* b>0 in eq.15) so that appearance of oxygen rotations *a priori* suppresses the ferroelectric distortion. In Ref. [162], Gu *et al.* have shown that, in $ZnSnO_3$, the higher-order coupling term $\emptyset^4P^2$ in eq. 15 has, however, a coefficient c < 0. This means that, although oxygen rotations and polarization indeed compete at small rotations amplitudes at which the $b\emptyset^2$ contribution dominates, they can nevertheless cooperate at large enough rotation amplitudes for which the negative $c\emptyset^4$ contribution to a_{eff} dominates. They further linked such dual nature of the interaction between oxygen rotations and polarization to steric effects. This highlights that in ABO_3 compounds showing small tolerance factors and large oxygen rotations, the latter can soften the polarization energy well and induce a ferroelectric instability through a so far overlooked cooperative anharmonic coupling ($c\emptyset^4P^2$). Since some of these compounds possibly exhibit magnetic properties, this opens a new route to identify promising candidates for multiferroism.

Such a progressive renormalization of the curvature of the polarization energy well by a non-polar distortion is reminiscent of the triggered mechanism proposed by Holakovsky[163]. However, in a "so-called" *triggered* ferroelectric phase transition, the destabilization of *P* has to be produced by a negative bi-quadratic coupling (b<0) to the primary order parameter while here it is linked to a higher-order term, which will affect the temperature behaviour and related properties. To keep the classification rigorous, we therefore prefer to speak here of a triggered-like transition. We notice that, to date, no example of a real triggered ferroelectric transition has been reported in simple ABO_3 perovskites. To our knowledge the only example of triggered structural phase transitions in simple perovskite is that recently highlighted in rare–earth nickelates $RNiO_3$ (R=Lu-Pr, Y), which concerns the triggering of a breathing distortion of the oxygen cages by oxygen rotations [164,165].

V. Spin, charge and orbital induce ferroelectricity

Up to now, we have addressed systems in which the ionic displacements drive the ferroelectric flavour of the material, irrespective of the proper or improper nature of the polarization. Such phenomenon in magnets produces what one often calls type I multiferroic compounds. However, there are other materials in which the electrons themselves produce the polarization. Although the polarization is often rather small in these compounds (of the order of few nC.cm^{-2}) with respect to that of "conventional" ferroelectrics (of the order of few μC.cm^{-2}), the strong coupling between *P* and the electronic structure (charge, spin or orbital degrees of freedom) warrants large magneto-electric responses. The electronic rather than ionic origin of *P* also potentially enables faster switching processes. DFT simulations, aiming at solving the electronic problem, are perfectly suited for studying electronically driven ferroelectrics. We present here the key results established on the basis of DFT simulations and we refer the reader to the reviews of Bousquet and Cano[92] as well as of Barone and Yamauchi[166] for further details.

1. Magnetically induced ferroelectricity

In some materials, often called type II multiferroics, the magnetic structure itself breaks the inversion symmetry and produces a spontaneous polarization. Such compounds are also called improper ferroelectrics since the polarization is not intrinsically unstable (single well in Fig. 1) but slave of another primary order parameter, which drive the polarization well to lower energy. Such a mechanism is similar to that explained in Section IV-1, except that, there, the primary order parameter was a non-polar lattice mode, while here it is related to the magnetic order.

An example of this type is the ↑↑↓↓ spin chains appearing in the (*ac*)-plane of the *Pbnm* structure of some rare-earth manganites $RMnO_3$ [167,168] (R=Lu, Tm, Er, Ho, Y). This magnetic order, also called E-AFM order (Figure 2.d), is based on nearest neighbor FM and next-nearest neighbor AFM interactions and it can break the inversion center of the *Pbnm* phase. DFT calculations performed by Picozzi *et al.* have provided a fundamental understanding in the origin of

ferroelectricity by demonstrating that the specific spin pattern produces different anion displacements according to the surrounding Mn spins (either ↑↑ or ↑↓) [169]. Assuming that B-O-B bond angles are smaller for AFM interactions than for FM interactions, the O displacements induced by spins are different according to the magnetic moment carried by surrounding B cations. For a FM trilinear chains (Figure 9.a), consecutive anions move with the same magnitude but in opposite direction. Consequently, there is no resultant electric dipole created. For a ↑↑↓ spin chain, anions move differently according to FM or AFM interactions, and their motions do not compensate. A resultant electrical dipole is created (Figure 9.b). Later on, model Hamiltonian based calculations highlighted the importance of the Jahn-Teller motion and orbital-ordering of the Mn^{3+} e_g electron on the ferroelectric properties of $HoMnO_3$ [170]. E-AFM order induced ferroelectricity was further validated experimentally in the orthorhombic polymorph of $YMnO_3$: using X-ray measurements, O displacements, of the order of 10^{-3} Å, are directly observed [171]. DFT studies also clarified the role of strain on the stability of the E-AFM order and on the polarization *P*[172], the effect of the chemical pressure (*i.e.* A site substitution) [173] or revealed a giant spin-driven polarization of the order of 1 μC.cm^{-2} in a phase achievable under high pressure[174].

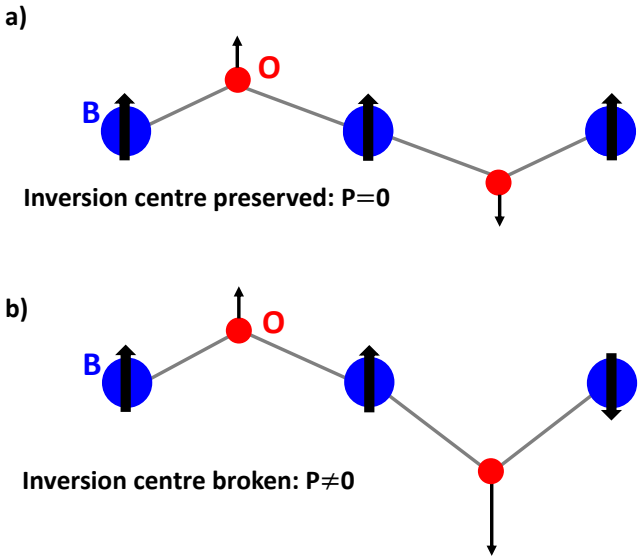

Figure 9: Illustration of anion displacements with respect of the neighboring B cation spins.

In 2009, extension of the E-AFM order with different stackings of the ↑↑↓↓ spin chains along the *b* axis of the *Pbnm* structure (S or T-type AFM orders, Figure 2.d) was also predicted on

the basis of DFT calculations to produce sizable spontaneous polarizations in $RNiO_3$ compounds [175] (R=Lu-Pr, Y). However, more recent works revealed that the magnetic structure of $RNiO_3$ compounds rather corresponds to $\uparrow 0 \downarrow 0$ spin chains due to disproportionation effects, thus not breaking the inversion center [176,177]. So far, there is no experimental report of ferroelectricity in rare-earth nickelates, but their experimental magnetic structure also remains elusive. We further notice that $YNiO_3$ shows a strong ferroelectric instability in its cubic phase (see Supplementary of Ref.[164]), but it is suppressed by more robust oxygen rotations of the oxygen octahedra bringing the system in the *Pbnm* phase discussed above.

Magnetically induced ferroelectricity can also appear in materials in which spin-orbit interaction (SOI) is playing a key role and produces non-collinear spin structures. This is the case, for instance, in $TbMnO_3$, a multiferroic compound displaying a non-collinear cycloidal spin structure of Mn^{3+} magnetic moments [5]. This peculiar magnetic order breaks the inversion centre and allows a small spontaneous polarization, further unlocking a large magneto-electric response. While the polarization was for a long time thought to originate from purely electronic effects, Malashevich and Vanderbilt as well as Xiang *et al.* demonstrated on the basis of DFT calculations including SOI that the ionic contributions to *P* is dominant over the pure electronic part [18,178,179]. DFT+SOI studies were also able to reproduce and explain the origin of the ferroelectric polarization in cuprates ($LiCu_2O_2$ and $LiCuVO_4$) exhibiting spin-spirals magnetic structures [180]. Apart from of ABO_3 materials, DFT also clarified the origin of the small polarization exhibited by $HoMn_2O_5$ and $TbMn_2O_5$ due to partly cancelling electronic and ionic contributions to *P* [181,182] while the polarization in YMn_2O_5 is purely electronic [183].

The polarization in type II multiferroics is not restricted to specific B site magnetic orders but it can be produced by the combination of magnetic orders on A and B sites cations (with or without SOI). For instance, a polarization enhancement is experimentally observed in $DyMnO_3$ once the Dy^{3+} magnetic moments order [184]. This was ascribed to the intimate coupling between *4f* and *3d* electrons *via* exchange-striction by DFT+U and DFT+hybrid calculations performed by Stroppa *et al.* in $DyFeO_3$ [53]. In 2017, Zhao *et al.* performed a systematic study of magnetically

induced ferroelectricity in $RCrO_3$ and $RFeO_3$ compounds (where R is a magnetic lanthanide) and observed that simple collinear orders on both A and B site cations, such as A-AFM, C-AFM or G-AFM orders, can give rise to "large" ferroelectric polarizations [185]. Again, a dominant non-relativist exchange-strictive mechanism is at the core of the spontaneous polarization. Finally, Senn and Bristowe used a group theory analysis to enumerate the possible coupling between magnetism and ferroelectricity in ABX_3 (X=O, F,…) perovskites [94].

2. ***Charge-order induced ferroelectricity***

By mixing cations with different valence states, one can achieve charge orderings in materials and create electronic polarization. This was formulated by Efremov, Van den Brink and Khomskii in 2004 [186,187] and realized in doped manganites [188] , with support from DFT to understand underlying mechanisms[189]. Although a non-perovskite, the most famous compound showing charge ordering is Fe_3O_4, also known as magnetite. This is the first magnetic compound discovered and it was known to develop ferroelectricity at low temperature since the eighties [190]. It is naturally based on two iron formal oxidations states, being 2+ and 3+ respectively, and on FeO_4 tetrahedrons[191]. DFT simulations performed by Picozzi *et al.* in 2009 were the first to reveal that the charge ordering between Fe^{3+} and Fe^{2+} breaks the inversion center and produces a spontaneous polarization in the compound [192]. The polarization was since measured and switched experimentally in thin films [193]. Due to its similarity with Fe_3O_4, the spinel $LuFe_2O_4$ in which Fe cations adopt 2+ and 3+ formal oxidation states was long time thought to be the prototypical charge order induced multiferroic compound [194]. However, a debate remains open regarding the ferroelectric properties of this material with a DFT study of 2008 predicting an anti-ferroelectric ground state [195].

Apart from explaining the origin of ferroelectricity in already known compounds, *first-principles* simulations also predicted a vanadium based spinel or other Fe based compounds to be good candidates for multiferroism [196–199]. Finally, Park *et al.* predicted in 2017 that $(La^{3+}VO_3)_1/(Sr^{2+}VO_3)_1$ (001)-oriented superlattices can exhibit a charge-ordered ground state in

which electron transfers between V^{3+} and V^{4+} cations produce an additional polarization orthogonal to that coming from the A cation ordering (*i.e.* coming from HIF) [200].

5. ***Orbital-order induced ferroelectricity***

Along with magnetism and charge ordering, orbitals can also produce a spontaneous polarization even though it is usually linked with or induced by magnetic or charge orderings, and thus the mechanisms remain more elusive. For instance, Varignon and coworkers showed that an electronic instability can produce an orbital ordering irrespective of a Jahn-Teller motion – which is just consequential – and produce a spontaneous electronic polarization of approximately 0.04 $\mu C.cm^{-2}$, reaching 0.34 $\mu C.cm^{-2}$ once the lattice relaxes, in 1/1 (001)-oriented superlattices based on $PrVO_3$ and $LaVO_3$ [137] (*i.e.* this electronic polarization is again orthogonal to that induced by HIF in similar spirit of the work of Park *et al.* [200]). Barone *et al.* proposed that an orbital-ordering is producing the electronic part of the polarization exhibited by undoped rare-earth manganites, although the origin of the orbital-order is likely due the specific E-AFM magnetic order [170]. Ultrathin films of $SrCrO_3$ have been predicted by Gupta *et al.* to become ferroelectric due to the appearance of an orbital ordering driven by lattice distortion [201]. Finally, a joint second-harmonic generation and DFT study revealed that a Jahn-Teller motion and its orbital ordering produce a B cation off-centering in some polar half-doped manganite thin films [202].

VI. Interfacial systems for efficient magneto-electrics

So far, we have focused on magneto-electric multiferroics combining ferroelectricity and magnetism within the same phase. Nevertheless, there is another route to achieve magneto-electricity: combine two materials exhibiting each only one of the desired properties and expect that the interface will exhibit the coupled functionality. In practice, two main strategies have been considered: (i) exploiting strain mediated coupling at the interface or (ii) harnessing the symmetry breaking occurring at the interface. The former route uses the strain coupling between a piezomagnetic and a piezoelectric material to enable a magneto-electric effect [203]. This strategy has the advantage that the effect can penetrate deep inside the film instead of being confined at the interface. The second strategy benefits from the symmetry breaking occurring at any interface: if one of the materials is a ferromagnet, then a magneto-electric effect is automatically allowed at the interface [204]. We emphasize that the inversion symmetry is also broken locally at the surface of a material that could also allow for magneto-electric effects. Since there are less constraints for realizing "interfacial systems", they have attracted a large interest both from theoretical and experimental points of view. Nevertheless, in this section, we only report selected discoveries to which *first-principles* simulations have contributed.

Modelling interfacial systems is challenging from the point of view of DFT simulations. Firstly, one must model metal-insulator capacitors under finite electric field. Secondly, DFT is well known for underestimating band gaps and thus band alignment at metal-insulator interfaces becomes a fundamental issue[12,205]. The first aspect was addressed by Stengel and co-workers during the late 2000's [205–207]. To better treat the band alignment problem, one could use beyond DFT methods such as DFT+U [208], although the choice of U parameters still has to be handled with care [209], or DFT+hybrid functionals better reproducing band gaps [208,210,211]. These problems are nowadays well understood and several key discoveries were enabled by DFT simulations [212].

1. Charge carrier mediated magneto-electric effect

The most striking advance unveiled by DFT simulations is the carrier mediated magneto-electric effect appearing at the $SrRuO_3/SrTiO_3$ interface [213]. In such a system, spin-polarized carriers of the metal accumulate or deplete at the interfacial region in order to screen the capacitive or bound charges at the interface under electric field (Figure 10). The effect is generic to any ferromagnetic (or any magnet) metal-dielectric interface and it should be enhanced at ferroelectric (*e.g.* $BaTiO_3$)-ferromagnetic metal interfaces [214]. Similar effects have been predicted by Tsymbal and co-workers at the surface of various metals such as CrO_2, Fe, Co or Ni under external electric field [215,216].

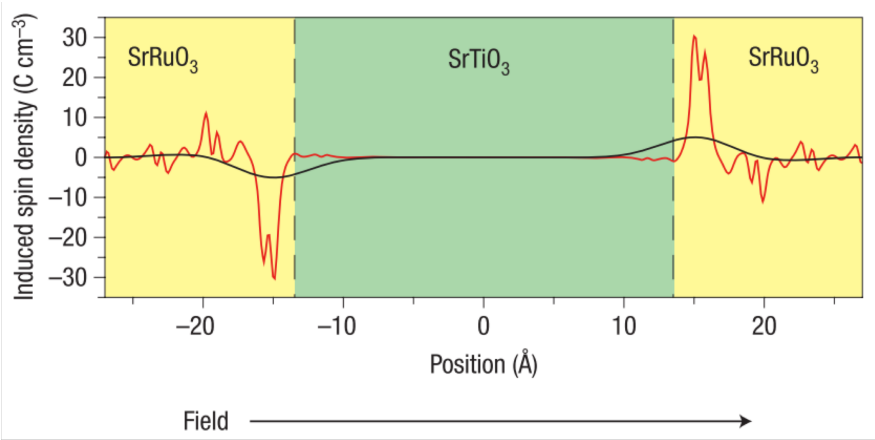

Figure 10: Planar (red) and microscopically averaged (black) charge in magnetic density at the interface between $SrTiO_3/SrRuO_3$ capacitor under an applied electric field. This figure is extracted from Ref. [213].

In the aim of realizing the predicted effects at Fe or Co surfaces, one can consider a hybrid system based on a ferroelectric perovskite and a metal. The $Fe/BaTiO_3$ is likely the most studied interfacial system in that respect. At the interface, Fe can induce a magnetic moment on Ti cations, whose magnitude directly depends on the orientation of the polarization in the ferroelectric [217–219] (Figure 11. a). DFT+U calculations from Lee *et al.* ascribed the mechanism underlying the interface magneto-electric effect to hybridization between Fe and Ti (see Figure 11) and carrier mediated processes [220]. Nearby the interface, the Ti *d* band peaks around 2 eV above the Fermi level (Figure 11.a) and it can interact with the minority levels of Fe (Figure 11.b). Fe-Ti hybridized *d* levels are created. The polarization then acts on the Fe-Ti distances and *de facto* on the level of hybridization and the resultant interfacial magnetic moment. Other

ferroelectric/metal interfaces have been investigated with *first-principles* simulations [208,218,221–223], including ferroelectric/antiferromagnetic metal interfaces[224].

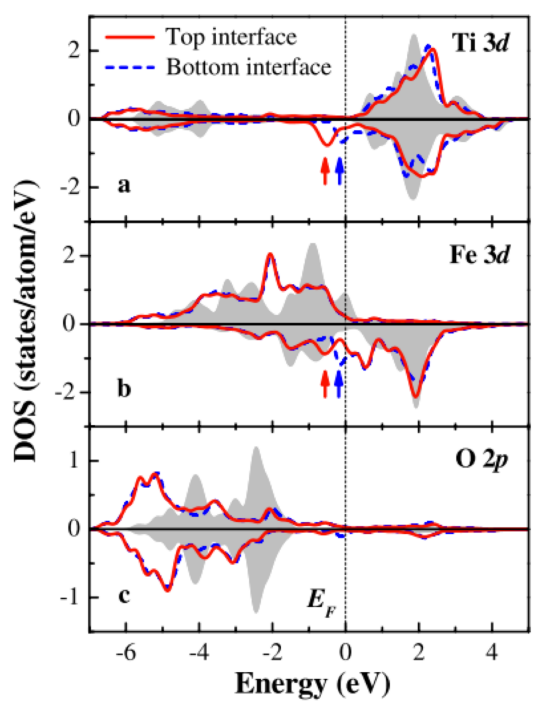

Figure 11: Projected density of states (pDOS) on Ti and Fe 3d levels (panels a and b, respectively) and O p levels (c) in the Fe/$BaTiO_3$ interfacial systems. Red and blue curves correspond to the system with a polarization pointing toward and away from the interface, respectively. Grey plots are the pDOS of central atoms. The Fermi level is located to E=0 eV. This figure is extracted from Ref.[217].

2. ***Ferroelectric control of magnetic order***

Along with tuning the amplitude of the induced magnetic moment, switching the orientation of the ferroelectric polarization can also change the magnetic order. Some systems such as doped manganites (*e.g.* $La_{1-x}A_xMnO_3$, A=Ca, Sr, Ba) exhibit a rich physical phase diagram as a function of the carrier concentration, and most notably the magnetic order can be altered by continuously changing the doping content. It is straightforward to seek for a ferroelectric control of carrier concentration and magnetic order in such systems. By putting $La_{1-x}A_xMnO_3$ (A=Ca, Sr, Ba) close to a transition, Burton and Tsymbal as well as Bristowe *et al.* demonstrated that reversing the polarization of the ferroelectric can switch the magnetic order of the manganite

from ferromagnetic to antiferromagnetic at $BaTiO_3/La_{1-x}A_xMnO_3$ interfaces [225,226]. More recently, a ferroelectric control of magnetism was observed at $BaTiO_3$/FeO interfaces covered with Co although the mechanism is rather different to carrier mediated effects [219]. DFT calculations of Plekhanov and Picozzi showed that depending on the orientation of the polarization in $BaTiO_3$, the Fe-O bond length at the FeO-TiO_2 interface as well as the Fe-O-Fe angles are dramatically altered which in turn tune the Fe-Fe magnetic interactions.

3. ***Ferroelectric control of magnetic easy axis, orbital occupancies and Curie temperature***

Another possibility to tune magnetic properties with the orientation of the ferroelectric polarization is to modify the magnetic easy axis, and *first-principles* simulations have been valuable in predicting this phenomenon [215,227–234]. In Fe/MgO [231] or other ferromagnetic metals such as (001)-oriented Ni, Fe or Ni [215,228], the modification of the magnetocrystalline anisotropy is attributed to changes of t_{2g} orbital occupancies due to the electric field. For Fe/ferroelectric oxide interfaces, modification of hybridization between Fe and Ti *d* levels are proposed to be the key factor [227].

Ferroelectricity is also a promising lever to tune orbital occupancies at ferroelectric/manganite interfaces [235]. Other interfacial systems such as short period $(BaTiO_3)_3/(La_{2/3}Sr_{1/3}MnO_3)_3$ superlattices were predicted and experimentally demonstrated to exhibit a strong enhancement of their Curie temperature [211]. Although the role of the polarization is not discussed, the large increase of T_c is assigned to an ordering of Mn orbitals created at the interface, that in turn increases orbital-overlaps and the strength of the double-exchange mechanism.

VII. Conclusions

In this article, we have highlighted various pathways to achieve magneto-electric compounds, focusing on the role played by DFT methods in boosting many discoveries. At the time of writing this article, advances in understanding and modelling perovskite materials are still on the rise, and most notably, strong dynamical electronic correlations that were believed to be the key aspect of *3d* ABO_3 compounds (to which belong the most famous multiferroic compounds) are demonstrated to a have marginal effects on the perovskite's properties [236]. It constitutes a significant advance in the search of novel multiferroic compounds by alleviating the computational cost for modelling such systems. So, DFT simulations combined with high-throughput methods [237–240], second-principles techniques and "inverse design" strategies [241] appear more than ever very promising to facilitate the discovery of ferroelectric ferromagnets showing large linear magneto-electric effect and operating at room temperature.

Acknowledgements

Ph.G acknowledges support from the F.R.S.-FNRS PDR project HiT4FiT, the ARC project AIMED and the ERA.NET project SIOX.

References

[1] P. Curie, J. Phys. **3**, 393 (1894).

[2] L.D. Landau and E.M. Lifshitz, *Electrodynamics of Continuous Media*, 2nd (Pergamon Press, 1958).

[3] M. Fiebig, J. Phys. D. Appl. Phys. **38**, R123 (2005).

[4] M. Bibes and A. Barthélémy, Nat. Mater. **7**, 425 (2008).

[5] T. Kimura, T. Goto, H. Shintani, K. Ishizaka, T. Arima, and Y. Tokura, Nature **426**, 55 (2003).

[6] N. Hur, S. Park, P.A. Sharma, J.S. Ahn, S. Guha, and S.W. Cheong, Nature **429**, 392 (2004).

[7] T. Goto, T. Kimura, G. Lawes, A.P. Ramirez, and Y. Tokura, Phys. Rev. Lett. **92**, 257201 (2004).

[8] W.F. Brown, R.M. Hornreich, and S. Shtrikman, Phys. Rev. **168**, 574 (1968).

[9] R.E. Cohen, Nature **358**, 136 (1992).

[10] D. Vanderbilt, Curr. Opin. Solid State Mater. Sci. **2**, 701 (1997).

[11] J. Junquera and P. Ghosez, Nature **422**, 506 (2003).

[12] J. Junquera and P. Ghosez, J. Comput. Theor. Nanosci. **5**, 2071 (2008).

[13] M. Dawber, K.M. Rabe, and J.F. Scott, Rev. Mod. Phys. **77**, 1083 (2005).

[14] R. Seshadri and N.A. Hill, Chem. Mater. **13**, 2892 (2001).

[15] S. Krohns and P. Lunkenheimer, Phys. Sci. Rev. (2019).

[16] B.B. Van Aken, T.T.M. Palstra, A. Filippetti, and N.A. Spaldin, Nat. Mater. **3**, 164 (2004).

[17] C.J. Fennie and K.M. Rabe, Phys. Rev. B **72**, 100103 (2005).

[18] A. Malashevich and D. Vanderbilt, Eur. Phys. J. B **71**, 345 (2009).

[19] V.M. Goldschmidt, Naturwissenschaften **14**, 477 (1926).

[20] N.A. Hill, J. Phys. Chem. B **104**, 6694 (2000).

[21] P. Baettig and N.A. Spaldin, Appl. Phys. Lett. **86**, 12505 (2005).

[22] R. Nechache, C. Harnagea, L.-P. Carignan, O. Gautreau, L. Pintilie, M.P. Singh, D. Ménard, P. Fournier, M. Alexe, and A. Pignolet, J. Appl. Phys. **105**, 061621 (2009).

[23] R. Nechache, C. Harnagea, A. Pignolet, F. Normandin, T. Veres, L.-P. Carignan, and D. Ménard, Appl. Phys. Lett. **89**, (2006).

[24] S. Bhattacharjee, E. Bousquet, and P. Ghosez, Phys. Rev. Lett. **102**, 117602 (2009).

[25] P. Hohenberg and W. Kohn, Phys. Rev. **136**, B864 (1964).

[26] W. Kohn and L.J. Sham, Phys. Rev. **140**, A1133 (1965).

[27] R.M. Martin, *Electronic Structure : Basic Theory and Practical Methods* (Cambridge university press, 2004).

[28] R.D. King-Smith and D. Vanderbilt, Phys. Rev. B **47**, 1651 (1993).

[29] D. Vanderbilt and R.D. King-Smith, Phys. Rev. B **48**, 4442 (1993).

[30] R. Resta, Rev. Mod. Phys. **66**, 899 (1994).

[31] R. Resta, Ferroelectrics **136**, 51 (1992).

[32] M. Veithen, X. Gonze, and P. Ghosez, Phys. Rev. B **71**, 125107 (2005).

[33] N. Sai, K.M. Rabe, and D. Vanderbilt, Phys. Rev. B **66**, 104108 (2002).

[34] I. Souza, J. Íñiguez, and D. Vanderbilt, Phys. Rev. Lett. **89**, 117602 (2002).

[35] M. Stengel, N.A. Spaldin, and D. Vanderbilt, Nat. Phys. **5**, 304 (2009).

[36] T. Thonhauser, D. Ceresoli, D. Vanderbilt, and R. Resta, Phys. Rev. Lett. **95**, 137205 (2005).

[37] D. Xiao, J. Shi, and Q. Niu, Phys. Rev. Lett. **95**, 137204 (2005).

[38] R. Resta, J. Phys. Condens. Matter **22**, 123201 (2010).

[39] A. Malashevich, I. Souza, S. Coh, and D. Vanderbilt, New J. Phys. **12**, 53032 (2010).

[40] D. Ceresoli, U. Gerstmann, A.P. Seitsonen, and F. Mauri, Phys. Rev. B **81**, 60409 (2010).

[41] V.I. Anisimov, J. Zaanen, and O.K. Andersen, Phys. Rev. B **44**, 943 (1991).

[42] M. Cococcioni and S. De Gironcoli, Phys. Rev. B **71**, 035105 (2005).

[43] J.B. Morée and B. Amadon, Phys. Rev. B **98**, 205101 (2018).

[44] I.A. Kornev, S. Lisenkov, R. Haumont, B. Dkhil, and L. Bellaiche, Phys. Rev. Lett. **99**, 227602 (2007).

[45] and J.Z. A. I. Liechtenstein, V. I. Anisimov, Phys. Rev. B **52**, 5467 (1995).

[46] S.L. Dudarev, G.A. Botton, S.Y. Savrasov, C.J. Humphreys, and A.P. Sutton, Phys. Rev. B **57**, 1505 (1998).

[47] T.A. Mellan, F. Cora, R. Grau-Crespo, and S. Ismail-Beigi, Phys. Rev. B **92**, 85151 (2015).

[48] E. Bousquet and N. Spaldin, Phys. Rev. B **82**, 220402(R) (2010).

[49] C. Lee, W. Yang, and R.G. Parr, Phys. Rev. B **37**, 785 (1988).

[50] J. Heyd, G.E. Scuseria, and M. Ernzerhof, J. Chem. Phys. **118**, 8207 (2003).

[51] D.I. Bilc, R. Orlando, R. Shaltaf, G.M. Rignanese, J. Iniguez, and P. Ghosez, Phys. Rev. B **77**,

165107 (2008).

[52] A. Stroppa and S. Picozzi, Phys. Chem. Chem. Phys. **12**, 5405 (2010).

[53] A. Stroppa, M. Marsman, G. Kresse, and S. Picozzi, New J. Phys. **12**, (2010).

[54] J. Hong, A. Stroppa, J. Iñiguez, S. Picozzi, D. Vanderbilt, J. J. I\~iguez, S. Picozzi, and D. Vanderbilt, Phys. Rev. B **85**, 054417 (2012).

[55] A. Prikockyte, D. Bilc, P. Hermet, C. Dubourdieu, and P. Ghosez, Phys. Rev. B **84**, 214301 (2011).

[56] J. Varignon and P. Ghosez, Phys. Rev. B **87**, 140403 (2013).

[57] J. Varignon, D. Fontaine, E. Bousquet, N.C. Bristowe, and P. Ghosez, Nat. Commun. **6**, 1 (2015).

[58] J. Sun, A. Ruzsinszky, and J. Perdew, Phys. Rev. Lett. **115**, 036402 (2015).

[59] J. Varignon, M. Bibes, and A. Zunger, Submitted (2018).

[60] J.W. Furness, Y. Zhang, C. Lane, I.G. Buda, B. Barbiellini, R.S. Markiewicz, A. Bansil, and J. Sun, Commun. Phys. **1**, 11 (2018).

[61] J. Varignon, M. Bibes, and A. Zunger, ArXiv 1901.00425 (2019).

[62] A. Filippetti and N.A. Spaldin, Phys. Rev. B **67**, 125109 (2003).

[63] A. Gellé, J. Varignon, and M.-B. Lepetit, EPL (Europhysics Lett. **88**, 37003 (2009).

[64] M.B. Lepetit, Theor. Chem. Acc. **135**, 91 (2016).

[65] J. Varignon, S. Petit, A. Gellé, and M.B. Lepetit, J. Phys. Condens. Matter **25**, 496004 (2013).

[66] E. Bousquet, N.A. Spaldin, and K.T. Delaney, Phys. Rev. Lett. **106**, 107202 (2011).

[67] J. Iñiguez, Phys. Rev. Lett. **101**, 117201 (2008).

[68] J.C. Wojdeł and J. Íñiguez, Phys. Rev. Lett. **103**, 267205 (2009).

[69] A. Malashevich, S. Coh, I. Souza, and D. Vanderbilt, Phys. Rev. B **86**, 094430 (2012).

[70] A. Scaramucci, E. Bousquet, M. Fechner, M. Mostovoy, and N.A. Spaldin, Phys. Rev. Lett. **109**, 197203 (2012).

[71] A. Malashevich, S. Coh, I. Souza, and D. Vanderbilt, Phys. Rev. B - Condens. Matter Mater. Phys. **86**, 1 (2012).

[72] F. Ricci and E. Bousquet, **116**, 227601 (2016).

[73] N.A. Spaldin, M. Fechner, E. Bousquet, A. Balatsky, and L. Nordstr, Phys. Rev. B **88**, 094429

(2013).

[74] F. Thöle, M. Fechner, and N.A. Spaldin, Phys. Rev. B **93**, 195167 (2016).

[75] N. Tillack, J.R. Yates, and P.G. Radaelli, Phys. Rev. B **94**, 100405(R) (2016).

[76] M. Ackermann, L. Bohat, P. Becker, T. Lorenz, N. Leo, and M. Fiebig, Phys. Rev. B **92**, 094431 (2015).

[77] N.A. Spaldin, M. Fiebig, and M. Mostovoy, J. Phys. Condens. Matter **20**, 434203 (2008).

[78] Y. Gao, D. Vanderbilt, and D. Xiao, Phys. Rev. B **97**, 134423 (2018).

[79] M. Mostovoy, A. Scaramucci, N.A. Spaldin, and K.T. Delaney, Phys. Rev. Lett. **105**, 087202 (2010).

[80] S. Prosandeev, I.A. Kornev, and L. Bellaiche, Phys. Rev. B **83**, 020102(R) (2011).

[81] D. Rahmedov, D. Wang, J. Añiguez, and L. Bellaiche, Phys. Rev. Lett. **109**, 037207 (2012).

[82] W. Zhong, K. Rabe, and D. Vanderbilt, Phys. Rev. Lett. **73**, 1861 (1994).

[83] W. Zhong, M. Rabe, and D. Vanderbilt, Phys. Rev. B **52**, 6301 (1995).

[84] J.C. Wojdeł, P. Hermet, M.P. Ljungberg, P. Ghosez, and J. Íñiguez, J. Phys. Condens. Matter **25**, (2013).

[85] P. García-Fernández, J.C. Wojdel, J. Iniguez, and J. Junquera, Phys. Rev. B **93**, 195137 (2016).

[86] J.H. Haeni, P. Irvin, W. Chang, R. Uecker, P. Reiche, Y.L. Li, S. Choudhury, W. Tian, M.E. Hawley, B. Craigo, A.K. Tagantsev, X.Q. Pan, S.K. Streiffer, L.Q. Chen, S.W. Kirchoefer, J. Levy, and D.G. Schlom, Nature **430**, 758 (2004).

[87] P. Ghosez and J.M. Triscone, Nat. Mater. **10**, 269 (2011).

[88] K.M. Rabe, C.H. Ahn, and J.-M. Triscone, *Physics of Ferroelectrics* (2007).

[89] A.M. Glazer, Acta Crystallogr. Sect. B Struct. Crystallogr. Cryst. Chem. **28**, 3384 (1972).

[90] T. Günter, E. Bousquet, A. David, P. Boullay, P. Ghosez, W. Prellier, and M. Fiebig, Phys. Rev. B **85**, 214120 (2012).

[91] E. Bousquet and N. Spaldin, Phys. Rev. Lett. **107**, 197603 (2011).

[92] E. Bousquet and A. Cano, J. Phys. Condens. Matter **28**, 123001 (2016).

[93] L. Bellaiche, Z. Gui, and I.A. Kornev, J. Phys. Condens. Matter **24**, 312201 (2012).

[94] M.S. Senn and N.C. Bristowe, Acta Crystallogr. Sect. A Found. Adv. **74**, 308 (2018).

[95] H. Béa, B. Dupé, S. Fusil, R. Mattana, E. Jacquet, B. Warot-Fonrose, F. Wilhelm, A. Rogalev, S.

Petit, V. Cros, A. Anane, F. Petroff, K. Bouzehouane, G. Geneste, B. Dkhil, S. Lisenkov, I. Ponomareva, L. Bellaiche, M. Bibes, and A. Barthélémy, Phys. Rev. Lett. **102**, 217603 (2009).

[96] O. Diéguez, O.E. González-Vázquez, J.C. Wojdeł, and J. Íñiguez, Phys. Rev. B **83**, 094105 (2011).

[97] Y. Yang, W. Ren, M. Stengel, X.H. Yan, and L. Bellaiche, Phys. Rev. Lett. **109**, 57602 (2012).

[98] Y. Yang, J. Íñiguez, A.J. Mao, and L. Bellaiche, Phys. Rev. Lett. **112**, 057202 (2014).

[99] J. Varignon, N.C. Bristowe, and P. Ghosez, Phys. Rev. Lett. **116**, 57602 (2016).

[100] G. Song and W. Zhang, Sci. Rep. **4**, 04564 (2014).

[101] P. Aguado-Puente, P. García-Fernández, and J. Junquera, Phys. Rev. Lett. **107**, 217601 (2011).

[102] E. Bousquet, N.A. Spaldin, and P. Ghosez, Phys. Rev. Lett. **104**, 037601 (2010).

[103] A.C. Garcia-Castro, N.A. Spaldin, A.H. Romero, and E. Bousquet, Phys. Rev. B **89**, 104107 (2014).

[104] A.C. Garcia-Castro, A.H. Romero, and E. Bousquet, Phys. Rev. Lett. **116**, 117202 (2016).

[105] U. Aschauer, R. Pfenninger, S.M. Selbach, T. Grande, and N.A. Spaldin, Phys. Rev. B **88**, 054111 (2013).

[106] R.U. Chandrasena, W. Yang, Q. Lei, M.U. Delgado-Jaime, K.D. Wijesekara, M. Golalikhani, B.A. Davidson, E. Arenholz, K. Kobayashi, M. Kobata, F.M.F. De Groot, U. Aschauer, N.A. Spaldin, X. Xi, and A.X. Gray, Nano Lett. **17**, 794 (2017).

[107] O. Copie, J. Varignon, H. Rotella, G. Steciuk, P. Boullay, A. Pautrat, A. David, B. Mercey, P. Ghosez, and W. Prellier, Adv. Mater. **29**, 1604112 (2017).

[108] S. V Kalinin and N.A. Spaldin, **858**, 858 (2014).

[109] T. Xu, T. Shimada, Y. Araki, J. Wang, and T. Kitamura, Phys. Rev. B **92**, 104106 (2015).

[110] J.C. Wojdeł and J. Íñiguez, Phys. Rev. Lett. **105**, 1 (2010).

[111] W. Baltensperger, J. Appl. Phys. **41**, 1052 (1970).

[112] R.F. Sabiryanov and S.S. Jaswal, Phys. Rev. Lett. **83**, 2062 (1999).

[113] C.J. Fennie and K.M. Rabe, Phys. Rev. Lett. **97**, 267602 (2006).

[114] J.H. Lee, L. Fang, E. Vlahos, X. Ke, Y.W. Jung, L.F. Kourkoutis, J.W. Kim, P.J. Ryan, T. Heeg, M. Roeckerath, V. Goian, M. Bernhagen, R. Uecker, P.C. Hammel, K.M. Rabe, S. Kamba, J. Schubert, J.W. Freeland, D.A. Muller, C.J. Fennie, P. Schiffer, V. Gopalan, E. Johnston-Halperin, and D.G. Schlom, Nature **466**, 954 (2010).

[115] J.H. Lee and K.M. Rabe, Phys. Rev. Lett. **104**, 2 (2010).

[116] V. Srinu Bhadram, B. Rajeswaran, A. Sundaresan, and C. Narayana, Eur. Phys. Lett. **101**, 17008 (2013).

[117] S. Petit, F. Moussa, M. Hennion, S. Pailhès, L. Pinsard-Gaudart, and A. Ivanov, Phys. Rev. Lett. **99**, 266604 (2007).

[118] M.K. Gupta, R. Mittal, M. Zbiri, N. Sharma, S. Rols, H. Schober, and S.L. Chaplot, J. Mater. Chem. C **3**, 11717 (2015).

[119] R. Schleck, Y. Nahas, R.P.S.M. Lobo, J. Varignon, M.B. Lepetit, C.S. Nelson, and R.L. Moreira, Phys. Rev. B **82**, 054412 (2010).

[120] N.A. Benedek and C.J. Fennie, J. Phys. Chem. C **117**, 13339 (2013).

[121] T.H. Kim, D. Puggioni, Y. Yuan, L. Xie, H. Zhou, N. Campbell, P.J. Ryan, Y. Choi, J.W. Kim, J.R. Patzner, S. Ryu, J.P. Podkaminer, J. Irwin, Y. Ma, C.J. Fennie, M.S. Rzchowski, X.Q. Pan, V. Gopalan, J.M. Rondinelli, and C.B. Eom, Nature **533**, 68 (2016).

[122] A.P.L. and D.G. Sannikov, Sov. Phys. Uspekhi **17**, 199 (1974).

[123] N. Sai, C.J. Fennie, and A.A. Demkov, Phys. Rev. Lett. **102**, 107601 (2009).

[124] M. Stengel, C.J. Fennie, and P. Ghosez, Phys. Rev. B - Condens. Matter Mater. Phys. **86**, 094112(R) (2012).

[125] S. Kamba, D. Nuzhnyy, M. Savinov, P. Tolédano, V. Laguta, P. Brázda, L. Palatinus, F. Kadlec, F. Borodavka, C. Kadlec, P. Bednyakov, V. Bovtun, M. Kempa, D. Kriegner, J. Drahokoupil, J. Kroupa, J. Prokleška, K. Chapagain, B. Dabrowski, and V. Goian, Phys. Rev. B **95**, 1 (2017).

[126] K. Xu, X.Z. Lu, and H. Xiang, Npj Quantum Mater. **2**, 1 (2017).

[127] J. Young and J.M. Rondinelli, Phys. Rev. B **89**, 2 (2014).

[128] J.M. Rondinelli and C.J. Fennie, Adv. Mater. **24**, 1961 (2012).

[129] E. Bousquet, M. Dawber, N. Stucki, C. Lichtensteiger, P. Hermet, S. Gariglio, J.M. Triscone, and P. Ghosez, Nature **452**, 732 (2008).

[130] N.A. Benedek and C.J. Fennie, Phys. Rev. Lett. **106**, 107204 (2011).

[131] H. Zhang, Y. Weng, X. Yao, and S. Dong, **91**, 195145 (2015).

[132] Q. Zhou and K.M. Rabe, ArXiv Prepr. ArXiv1306.1839 (2013).

[133] A. Stroppa, P. Barone, P. Jain, J.M. Perez-Mato, and S. Picozzi, Adv. Mater. **25**, 2284 (2013).

[134] A. Stroppa, P. Jain, P. Barone, M. Marsman, J.M. Perez-Mato, A.K. Cheetham, H.W. Kroto, and S. Picozzi, Angew. Chemie - Int. Ed. **50**, 5847 (2011).

[135] J. Young, A. Stroppa, S. Picozzi, and J.M. Rondinelli, Dalt. Trans. **44**, 10644 (2015).

[136] H.J. Zhao, W. Ren, Y. Yang, J. Íñiguez, X.M. Chen, and L. Bellaiche, Nat. Commun. **5**, 4021 (2014).

[137] J. Varignon, N.C. Bristowe, E. Bousquet, and P. Ghosez, Sci. Rep. **5**, 15364 (2015).

[138] A. Cammarata and J.M. Rondinelli, **014102**, 1 (2015).

[139] C. Xu, Y. Li, B. Xu, J. Íñiguez, W. Duan, and L. Bellaiche, Adv. Funct. Mater. **27**, 1604513 (2017).

[140] Y. Tian, A. Stroppa, Y.S. Chai, P. Barone, M. Perez-Mato, S. Picozzi, and Y. Sun, Phys. Status Solidi - Rapid Res. Lett. **9**, 62 (2015).

[141] X.Q. Liu, J.W. Wu, X.X. Shi, H.J. Zhao, H.Y. Zhou, R.H. Qiu, W.Q. Zhang, and X.M. Chen, Appl. Phys. Lett. **106**, 202903 (2015).

[142] M.S. Senn, A. Bombardi, C.A. Murray, C. Vecchini, A. Scherillo, X. Luo, and S.W. Cheong, Phys. Rev. Lett. **114**, 035701 (2015).

[143] H. Sim and B.G. Kim, Phys. Rev. B - Condens. Matter Mater. Phys. **89**, 144114 (2014).

[144] N.A. Benedek, Inorg. Chem. **53**, 3769 (2014).

[145] C. Dixon, J. McNulty, K. Knight, A. Gibbs, and P. Lightfoot, Crystals **7**, 135 (2017).

[146] N.A. Benedek, J.M. Rondinelli, H. Djani, P. Ghosez, and P. Lightfoot, Dalt. Trans. **44**, 10543 (2015).

[147] Y.S. Oh, X. Luo, F.T. Huang, Y. Wang, and S.W. Cheong, Nat. Mater. **14**, 407 (2015).

[148] M.J. Pitcher, P. Mandal, M.S. Dyer, J. Alaria, P. Borisov, H. Niu, J.B. Claridge, and M.J. Rosseinsky, Science (80-.). **347**, 420 (2015).

[149] H.L.B. Boström, M.S. Senn, and A.L. Goodwin, Nat. Commun. **9**, 2380 (2018).

[150] A.T. Mulder, N.A. Benedek, J.M. Rondinelli, and C.J. Fennie, Adv. Funct. Mater. **23**, 4810 (2013).

[151] H.J. Zhao, J. Íñiguez, W. Ren, X.M. Chen, and L. Bellaiche, Phys. Rev. B **89**, 1 (2014).

[152] I. Etxebarria, J.M. Perez-Mato, and P. Boullay, Ferroelectrics **401**, 17 (2010).

[153] F. Ye, J. Wang, J. Sheng, C. Hoffmann, T. Gu, H.J. Xiang, W. Tian, J.J. Molaison, A.M. Santos,

M. Matsuda, B.C. Chakoumakos, X. Tong, B. Gao, J.W. Kim, and S. Cheong, Phys Rev B **97**, 041112 (2018).

[154] J. Zhang, L. Lin, Y. Zhang, M. Wu, B.I. Yakobson, and S. Dong, J. Am. Chem. Soc. **140**, 9768 (2018).

[155] J. Peng, Y. Zhang, L. Lin, L. Lin, and M. Liu, J. Phys. D. Appl. Phys. **51**, 243002 (2018).

[156] S. Dong, H. Xiang, and E. Dagotto, ArXiv **1902.01532**, 1 (n.d.).

[157] B. Xu, D. Wang, H.J. Zhao, J. Íñiguez, X.M. Chen, and L. Bellaiche, Adv. Funct. Mater. **25**, 3626 (2015).

[158] E.A. Nowadnick and C.J. Fennie, Phys. Rev. B **94**, 104105 (2016).

[159] Z. Zanolli, J.C. Wojdeł, J. Íñiguez, and P. Ghosez, Phys. Rev. B **88**, 060102(R) (2013).

[160] K.I. Kugel and D.I. Khomskii, Sov. Phys. JETP **64**, 1429 (1973).

[161] A.C. Garcia-Castro, W. Ibarra-Hernandez, E. Bousquet, and A.H. Romero, Phys. Rev. Lett. **121**, 117601 (2018).

[162] T. Gu, T. Scarbrough, Y. Yang, J. Íñiguez, L. Bellaiche, and H.J. Xiang, Phys. Rev. Lett. **120**, 197602 (2018).

[163] J. Holakovsky, Phys. Status Solidi **56**, 615 (1973).

[164] A. Mercy, J. Bieder, J. Íñiguez, and P. Ghosez, Nat. Commun. **8**, 1677 (2017).

[165] R.J. Green, K. Müller-caspary, I. Lobato, L. Li, V. Aert, J. Verbeeck, M. Huijben, M.N. Grisolia, V. Rouco, R. El Hage, J.E. Villegas, A. Mercy, M. Bibes, P. Ghosez, G.A. Sawatzky, Z. Liao, N. Gauquelin, R.J. Green, K. Müller-caspary, I. Lobato, and L. Li, **115**, (2018).

[166] K. Yamauchi and P. Barone, J. Phys. Condens. Matter **26**, 103201 (2014).

[167] A. Muñoz, M.T. Casais, J.A. Alonso, M.J. Martínez-Lope, J.L. Martinez, and M.T. Fernandez-Diaz, Inorg. Chem. **40**, 1020 (2001).

[168] J.S. Zhou and J.B. Goodenough, Phys. Rev. Lett. **96**, 247202 (2006).

[169] S. Picozzi, K. Yamauchi, B. Sanyal, I.A. Sergienko, and E. Dagotto, Phys. Rev. Lett. **99**, 227201 (2007).

[170] P. Barone, K. Yamauchi, and S. Picozzi, Phys. Rev. Lett. **106**, 077201 (2011).

[171] D. Okuyama, S. Ishiwata, Y. Takahashi, K. Yamauchi, S. Picozzi, K. Sugimoto, H. Sakai, M. Takata, R. Shimano, Y. Taguchi, T. Arima, and Y. Tokura, Phys. Rev. B **84**, 054440 (2011).

[172] D. Iuşan, K. Yamauchi, P. Barone, B. Sanyal, O. Eriksson, G. Profeta, and S. Picozzi, Phys. Rev. B - Condens. Matter Mater. Phys. **87**, 014403 (2013).

[173] K. Yamauchi, F. Freimuth, S. Blügel, and S. Picozzi, Phys. Rev. B **78**, 104403 (2008).

[174] T. Aoyama, K. Yamauchi, A. Iyama, S. Picozzi, K. Shimizu, and T. Kimura, Nat. Commun. **5**, 4927 (2014).

[175] G. Giovannetti, S. Kumar, D. Khomskii, S. Picozzi, and J. Van Den Brink, Phys. Rev. Lett. **103**, 156401 (2009).

[176] H. Park, A.J. Millis, and C.A. Marianetti, Phys. Rev. Lett. **109**, 1 (2012).

[177] J. Varignon, M.N. Grisolia, J. Íñiguez, A. Barthélémy, and M. Bibes, Npj Quantum Mater. **2**, 21 (2017).

[178] A. Malashevich and D. Vanderbilt, Phys. Rev. Lett. **101**, 037210 (2008).

[179] H.J. Xiang, S.H. Wei, M.H. Whangbo, and J.L.F. Da Silva, Phys. Rev. Lett. **101**, 037209 (2008).

[180] H.J. Xiang and M.H. Whangbo, Phys. Rev. Lett. **99**, 257203 (2007).

[181] T.R. Chang, H.T. Jeng, C.Y. Ren, and C.S. Hsue, Phys. Rev. B **84**, 024421 (2011).

[182] G. Giovannetti and J. Van Den Brink, Phys. Rev. Lett. **100**, 227603 (2008).

[183] S. Partzsch, S.B. Wilkins, J.P. Hill, E. Schierle, E. Weschke, D. Souptel, B. Büchner, and J. Geck, Phys. Rev. Lett. **107**, 057201 (2011).

[184] O. Prokhnenko, R. Feyerherm, E. Dudzik, S. Landsgesell, N. Aliouane, L.C. Chapon, and D.N. Argyriou, Phys. Rev. Lett. **98**, 057206 (2007).

[185] H.J. Zhao, L. Bellaiche, X.M. Chen, and J. Íñiguez, Nat. Commun. **8**, 14025 (2017).

[186] D. V. Efremov, J. Van Den Brink, and D.I. Khomskii, Nat. Mater. **3**, 853 (2004).

[187] C. Ederer and N.A. Spaldin, Nat. Mater. **3**, 849 (2004).

[188] A.M. Kadomtseva, Y.F. Popov, G.P. Vorob'ev, K.I. Kamilov, V.Y. Ivanov, A.A. Mukhin, and A.M. Balbashov, J. Exp. Theor. Phys. **106**, 130 (2008).

[189] G. Giovannetti, S. Kumar, J. Van Den Brink, and S. Picozzi, Phys. Rev. Lett. **103**, 037601 (2009).

[190] K. Kato, S. Iida, K. Yanai, and K. Mizushima, J. Magn. Magn. Mater. **31**–**34**, 783 (1983).

[191] M.S. Senn, J.P. Wright, and J.P. Attfield, Nature **481**, 173 (2012).

[192] K. Yamauchi, T. Fukushima, and S. Picozzi, Phys. Rev. B **79**, 212404 (2009).

[193] M. Alexe, M. Ziese, D. Hesse, P. Esquinazi, K. Yamauchi, T. Fukushima, S. Picozzi, and U.

Gösele, Adv. Mater. **21**, 4452 (2009).

[194] N. Ikeda, H. Ohsumi, K. Ohwada, K. Ishii, T. Inami, K. Kakurai, Y. Murakami, K. Yoshii, S. Mori, Y. Horibe, and H. Kitô, Nature **436**, 1136 (2005).

[195] M. Angst, R.P. Hermann, A.D. Christianson, M.D. Lumsden, C. Lee, M.H. Whangbo, J.W. Kim, P.J. Ryan, S.E. Nagler, W. Tian, R. Jin, B.C. Sales, and D. Mandrus, Phys. Rev. Lett. **101**, 227601 (2008).

[196] G. Giovannetti, A. Stroppa, S. Picozzi, D. Baldomir, V. Pardo, S. Blanco-Canosa, F. Rivadulla, S. Jodlauk, D. Niermann, J. Rohrkamp, T. Lorenz, S. Streltsov, D.I. Khomskii, and J. Hemberger, Phys. Rev. B **83**, 060402(R) (2011).

[197] K. Yamauchi, T. Oguchi, and S. Picozzi, J. Phys. Soc. Japan **83**, 094712 (2014).

[198] L.-F. Lin, Q.-R. Xu, Y. Zhang, J.-J. Zhang, Y.-P. Liang, and S. Dong, Phys. Rev. Mater. **1**, 071401 (2017).

[199] K. Yamauchi and S. Picozzi, Phys. Rev. Lett. **105**, 107202 (2010).

[200] S.Y. Park, A. Kumar, and K.M. Rabe, Phys. Rev. Lett. **118**, 087602 (2017).

[201] K. Gupta, P. Mahadevan, P. Mavropoulos, and M. Ležaić, Phys. Rev. Lett. **111**, 077601 (2013).

[202] N. Ogawa, Y. Ogimoto, Y. Ida, Y. Nomura, R. Arita, and K. Miyano, Phys. Rev. Lett. **108**, 157603 (2012).

[203] H. Zheng, J. Wang, S.E. Lofland, Z. Ma, L. Mohaddes-Ardabili, T. Zhao, L. Salamanca-Riba, S.R. Shinde, S.B. Ogale, F. Bai, D. Viehland, Y. Jia, D.G. Schlom, M. Wuttig, A. Roytburd, and R. Ramesh, Science (80-.). **303**, 661 (2004).

[204] H. Yamada, Y. Ogawa, Y. Ishii, H. Sato, M. Kawasaki, H. Akoh, and Y. Tokura, Science (80-.). **305**, 646 (2004).

[205] M. Stengel, P. Aguado-Puente, N.A. Spaldin, and J. Junquera, Phys. Rev. B **83**, 235112 (2011).

[206] M. Stengel and N.A. Spaldin, Phys. Rev. B - Condens. Matter Mater. Phys. **75**, 205121 (2007).

[207] M. Stengel and N.A. Spaldin, Nature **443**, 679 (2006).

[208] D. Di Sante, K. Yamauchi, and S. Picozzi, J. Phys. Condens. Matter **25**, 066001 (2013).

[209] H. Chen and S. Ismail-Beigi, Phys. Rev. B - Condens. Matter Mater. Phys. **86**, 024433 (2012).

[210] A.B. Koçak, J. Varignon, S. Lemal, P. Ghosez, and M.B. Lepetit, Phys. Rev. B **96**, 125155 (2017).

[211] A. Sadoc, B. Mercey, C. Simon, D. Grebille, W. Prellier, and M.B. Lepetit, Phys. Rev. Lett. **104**,

046804 (2010).

[212] R. Ramesh, Nat. Nanotechnol. **3**, 7 (2008).

[213] J.M. Rondinelli, M. Stengel, and N.A. Spaldin, Nat. Nanotechnol. **3**, 46 (2008).

[214] M.K. Niranjan, J.D. Burton, J.P. Velev, S.S. Jaswal, and E.Y. Tsymbal, Appl. Phys. Lett. **95**, 05250 (2009).

[215] N. Bonfoh, S. Tiem, and P. Lipinski, Phys. Rev. Lett. **41**, 137201 (2007).

[216] C.G. Duan, C.W. Nan, S.S. Jaswal, and E.Y. Tsymbal, Phys. Rev. B **79**, 140403(R) (2009).

[217] C.G. Duan, S.S. Jaswal, and E.Y. Tsymbal, Phys. Rev. Lett. **97**, 047201 (2006).

[218] M. Fechner, I. V. Maznichenko, S. Ostanin, A. Ernst, J. Henk, P. Bruno, and I. Mertig, Phys. Rev. B **78**, 212406 (2008).

[219] G. Radaelli, D. Petti, E. Plekhanov, I. Fina, P. Torelli, B.R. Salles, M. Cantoni, C. Rinaldi, D. Gutiérrez, G. Panaccione, M. Varela, S. Picozzi, J. Fontcuberta, and R. Bertacco, Nat. Commun. **5**, 3404 (2014).

[220] J. Lee, N. Sai, T. Cai, Q. Niu, and A.A. Demkov, Phys. Rev. B **81**, 144425 (2010).

[221] M.K. Niranjan, J.P. Velev, C.-G. Duan, S.S. Jaswal, and E.Y. Tsymbal, Phys. Rev. B **78**, 104405 (2008).

[222] K. Yamauchi, B. Sanyal, and S. Picozzi, Appl. Phys. Lett. **91**, 062506 (2007).

[223] M. Hölzer, M. Fechner, S. Ostanin, and I. Mertig, J. Phys. Condens. Matter **23**, 455902 (2011).

[224] E. Plekhanov, A. Stroppa, and S. Picozzi, J. Appl. Phys. **120**, 074104 (2016).

[225] J.D. Burton and E.Y. Tsymbal, Phys. Rev. B **80**, 174406 (2009).

[226] N.C. Bristowe, M. Stengel, P.B. Littlewood, J.M. Pruneda, and E. Artacho, Phys. Rev. B **85**, 024106 (2012).

[227] C.G. Duan, J.P. Velev, R.F. Sabirianov, W.N. Mei, S.S. Jaswal, and E.Y. Tsymbal, Appl. Phys. Lett. **92**, 122905 (2008).

[228] K. Nakamura, R. Shimabukuro, Y. Fujiwara, T. Akiyama, T. Ito, and A.J. Freeman, Phys. Rev. Lett. **102**, 187201 (2009).

[229] M. Tsujikawa and T. Oda, Phys. Rev. Lett. **102**, 247203 (2009).

[230] P. V. Lukashev, J.D. Burton, S.S. Jaswal, and E.Y. Tsymbal, J. Phys. Condens. Matter **24**, 226003 (2012).

[231] M.K. Niranjan, C.G. Duan, S.S. Jaswal, and E.Y. Tsymbal, Appl. Phys. Lett. **96**, 222504 (2010).

[232] H. Zhang, M. Richter, K. Koepernik, I. Opahle, F. Tasnádi, and H. Eschrig, New J. Phys. **11**, 043007 (2009).

[233] M. Lee, H. Choi, and Y.C. Chung, J. Appl. Phys. **113**, 17C729 (2013).

[234] M. Fechner, P. Zahn, S. Ostanin, M. Bibes, and I. Mertig, Phys. Rev. Lett. **108**, 197206 (2112).

[235] H. Chen, Q. Qiao, M.S.J. Marshall, A.B. Georgescu, A. Gulec, P.J. Phillips, R.F. Klie, F.J. Walker, C.H. Ahn, and S. Ismail-Beigi, Nano Lett. **14**, 4965 (2014).

[236] J. Varignon, M. Bibes, and A. Zunger, Nat. Commun. **10**, 1658 (2019).

[237] W. Setyawan and S. Curtarolo, Comput. Mater. Sci. **49**, 299 (2010).

[238] G. Hautier, A. Jain, and S.P. Ong, J. Mater. Sci. **47**, 7317 (2012).

[239] A. Jain, S.P. Ong, G. Hautier, W. Chen, W.D. Richards, S. Dacek, S. Cholia, D. Gunter, D. Skinner, G. Ceder, and K. a. Persson, APL Mater. **1**, 011002 (2013).

[240] J.W. Bennett, K.F. Garrity, K.M. Rabe, and D. Vanderbilt, Phys. Rev. Lett. **109**, 167602 (2012).

[241] A. Zunger, Nat. Rev. Chem. **2**, 121 (2018).